

THE DISCRIMINATIVE FUNCTIONAL MIXTURE MODEL FOR A COMPARATIVE ANALYSIS OF BIKE SHARING SYSTEMS

BY CHARLES BOUVEYRON, ETIENNE CÔME AND JULIEN JACQUES

Université Paris Descartes, IFSTTAR and Université Lumière Lyon 2

Bike sharing systems (BSSs) have become a means of sustainable intermodal transport and are now proposed in many cities worldwide. Most BSSs also provide open access to their data, particularly to real-time status reports on their bike stations. The analysis of the mass of data generated by such systems is of particular interest to BSS providers to update system structures and policies. This work was motivated by interest in analyzing and comparing several European BSSs to identify common operating patterns in BSSs and to propose practical solutions to avoid potential issues. Our approach relies on the identification of common patterns between and within systems. To this end, a model-based clustering method, called FunFEM, for time series (or more generally functional data) is developed. It is based on a functional mixture model that allows the clustering of the data in a discriminative functional subspace. This model presents the advantage in this context to be parsimonious and to allow the visualization of the clustered systems. Numerical experiments confirm the good behavior of FunFEM, particularly compared to state-of-the-art methods. The application of FunFEM to BSS data from JCDecaux and the Transport for London Initiative allows us to identify 10 general patterns, including pathological ones, and to propose practical improvement strategies based on the system comparison. The visualization of the clustered data within the discriminative subspace turns out to be particularly informative regarding the system efficiency. The proposed methodology is implemented in a package for the R software, named `funFEM`, which is available on the CRAN. The package also provides a subset of the data analyzed in this work.

1. Introduction. This work was motivated by the will to analyze and compare bike sharing systems (BSSs) to identify their common strengths and weaknesses. This type of study is possible because most BSS operators, in dozens of cities worldwide, provide open access to real-time status reports

Received July 2014; revised April 2015.

Key words and phrases. Model-based clustering, functional data, dimension reduction, open data, bike sharing systems.

This is an electronic reprint of the original article published by the Institute of Mathematical Statistics in *The Annals of Applied Statistics*, 2015, Vol. 9, No. 4, 1726–1760. This reprint differs from the original in pagination and typographic detail.

on their bike stations (e.g., the number of available bikes, the number of free bike stands). The implementation of bike sharing systems is one of the urban mobility services proposed in cities across the world as an additional means of sustainable intermodal transport. Several studies [Froehlich, Neumann and Oliver (2009), Borgnat et al. (2011), Vogel and Mattfeld (2011), Lathia, Saniul and Capra (2012)] have shown the usefulness of analyzing the data collected by BSS operators and city authorities. A statistical analysis of these data helps in the development of new and innovative approaches for a better understanding of both urban mobility and BSS use. The design of BSSs, the adjustment of pricing policies and the improvement of system services (e.g., redistribution of bikes over stations) can all benefit from this type of analysis [Dell’Olio, Ibeas and Moura (2011), Lin and Yang (2011)].

However, the amount of data collected on such systems is often very large. It is therefore difficult to acquire knowledge using it without the help of automatic algorithms that extract mobility patterns and give a synthetic view of the information. This task is usually achieved in the literature using clustering approaches. In almost all clustering studies conducted until now, bicycle sharing stations are grouped according to their usage profiles, thus highlighting the relationships between time of day, location and usage. In this way, the global behavior of each station can be efficiently summarized using a few clusters. These data can be used afterward to analyze the effect of changing pricing policies or opening new sets of stations [Lathia, Saniul and Capra (2012)]. Clustering results can also be used to study the cause of network imbalance [Vogel and Mattfeld (2011), Vogel, Greiser and Mattfeld (2011), Côme and Oukhellou (2014)] and serve as a first step toward providing automatic reallocation strategies. In the same way, the clustered results can be used to compare the level of services reached by the systems of several cities through the inspection of the proportions of stations that belong to each cluster in the different cities.

From a methodological point of view, the first attempt in this line of work was made by Froehlich, Neumann and Oliver (2008), who analyzed a data set from the Barcelona Bicing system. The data correspond to station occupancy statistics in the form of free slots, available bikes over several time frames and other station activity statistics derived from station occupancy data collected every 5 minutes. The clustering is performed using a Gaussian mixture model based on features such as the average number of available bikes at different periods of the day. It should be noted that such techniques do not really take advantage of the temporal dynamic of data. In Froehlich, Neumann and Oliver (2009), two types of clustering are compared, both of which are performed by hierarchical aggregation. The first one uses activity statistics derived from the evolution of station occupancy, whereas the second directly uses the number of available bicycles throughout the day.

Other studies, such as Lathia, Saniul and Capra (2012), use similar clustering techniques and data. As in Froehlich, Neumann and Oliver (2009), each station is described by a time series vector that corresponds to the normalized available bicycle value of the station throughout the day. Each element of the feature vector is therefore equal to the number of available bicycles divided by the station size. These time series are then smoothed using a moving average and clustered using a hierarchical agglomerative algorithm [see page 552 of Duda, Hart and Stork (2001)], with a cosine distance. Another work that uses the same type of data was proposed by Vogel and Mattfeld (2011), Vogel, Greiser and Mattfeld (2011); it uses feature vectors to describe the stations that come from normalizing arrival and departure counts per hour and also handles weekdays and weekends separately. Classical clustering algorithms, that is, k -means, Gaussian mixture models and sequential information bottleneck (sIB), are then compared. Finally, Côme and Oukhellou (2014) recently proposed an original approach considering a generative model based on Poisson mixtures to cluster stations with respect to hourly usage profiles build from trip data. The results obtained for the Vélib’ system (Paris) were then analyzed with respect to the city geography and sociology.

However, all of these works share two limitative characteristics: They are limited to one BSS (one city), and they do not explicitly model the functional nature of the data. Indeed, the observed time series are clustered in those works using either geometric methods based on distances between time series or by creating features that summarize the activity in the given periods of the day (and thus omitting the temporal dynamics of the data). In this work, we aim to go beyond the analyses made in those works by comparing several European BSSs using a clustering approach designed for time series data. To this end, we introduce a novel model-based clustering method devoted to time series (and, more generally, functional data) that is able to take into account the nature of the BSS data. The proposed methodology, called FunFEM, is based on the discriminative functional mixture (DFM) model, which models the data into a single discriminative functional subspace. This subspace subsequently allows an insightful visualization of the clustered data and eases the comparison of systems regarding the identified patterns. A family of 12 models is also proposed by relaxing or constraining the main DFM model, allowing it to handle a wide range of situations. The FunFEM algorithm is proposed for the inference of the DFM models, and model selection can be performed either by BIC or the “slope heuristic.” In addition, the selection of the most discriminative basis functions can be made afterward by introducing sparsity through a ℓ_1 -type penalization. The comparison of 8 European BSS using FunFEM allows us to identify pathological and healthy patterns in the system dynamic and to propose practical improvement strategies based on the most efficient systems.

TABLE 1
*Summary statistics for the eight bike sharing systems involved
in the study*

City	Stations	Bikes
Paris	1230	18,000
London	740	9500
Lyon	345	3200
Bruxelles	330	3800
Valencia	280	2400
Sevilla	260	2150
Marseille	120	650
Nantes	102	880

The paper is organized as follows. Section 2 presents the BSS data used to analyze and compare several European bike sharing systems. Section 3 introduces the DFM model, its model family and the FunFEM algorithm. The model choice and selection of the discriminative functions are also discussed in Section 3. Numerical experiments on simulated and benchmark data sets are then presented in Section 4 to validate the proposed approach. Section 5 presents the analyses and comparisons of 8 bike sharing systems using the FunFEM algorithm. Based on the comparison results, recommendations to BSS providers and city planners are made. Finally, Section 6 provides concluding remarks.

2. The BSS data. In this work we want to analyze station occupancy data collected over the course of one month on eight bike sharing systems in Europe. The data were collected over 5 weeks, between February, 24 and March, 30, 2014. Table 1 lists the BSSs included in this study and some summary statistics on the systems. Figure 1 visualizes the locations of the studied systems. The cities were chosen to cover different cases in terms of the geographic positions of the city (south/north of Europe) and to cover a range of system sizes, from small-scale systems, such as Nantes, to much larger systems, such as Paris.

The station status information, in terms of available bikes and docks, were downloaded every hour during the study period for the seven systems from the open-data APIs provided by the JCDecaux company¹ and by the Transport for London initiative.² To accommodate the varying stations sizes (in

¹The real-time data are available at <https://developer.jcdecaux.com/> (with an api key).

²The real-time data are available at <https://www.tfl.gov.uk/info-for/open-data-users/> (with an api key).

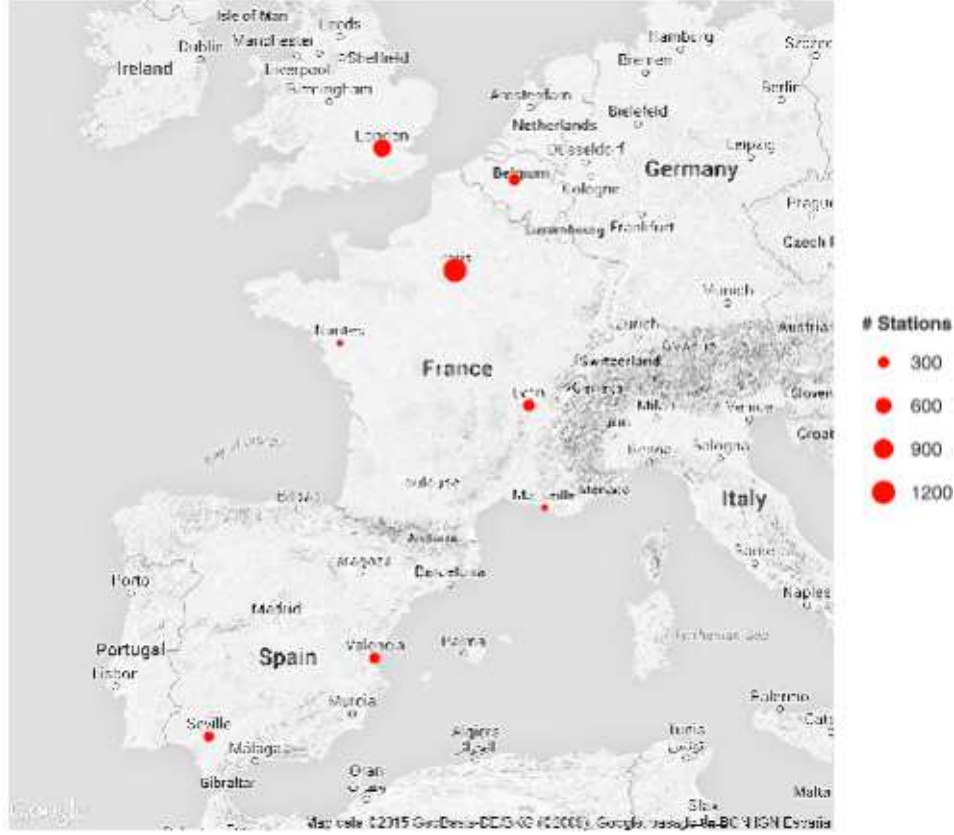


FIG. 1. Map of the eight European bike sharing systems involved in the study. The dot size denotes the system size.

terms of the number of docking points), we normalized the number of available bikes by the station size and obtained a loading profile for each station. The final data set contains 3230 loading profiles, one per station, sampled at 1448 time points. Notice that the sampling is not perfectly regular; there is an hour, on average, between the two sample points.

The daily and weekly habits of inhabitants introduce a periodic behavior in the BSS station loading profiles, with a natural period of one week. It is then natural to use a Fourier basis to smooth the curves, with basis functions corresponding to sine and cosine functions of periods equal to fractions of this natural period of the data. Using such a procedure, the profiles of the 3230 stations were projected on a basis of 41 Fourier functions (see Section 3 for details); the smoothed curves obtained for 6 different stations are depicted in Figure 2, together with the curve samples. A typical periodic behavior is clearly visible in this figure for some stations. Some other stations exhibit, however, a less clear pattern, such as curves 2, 4 and

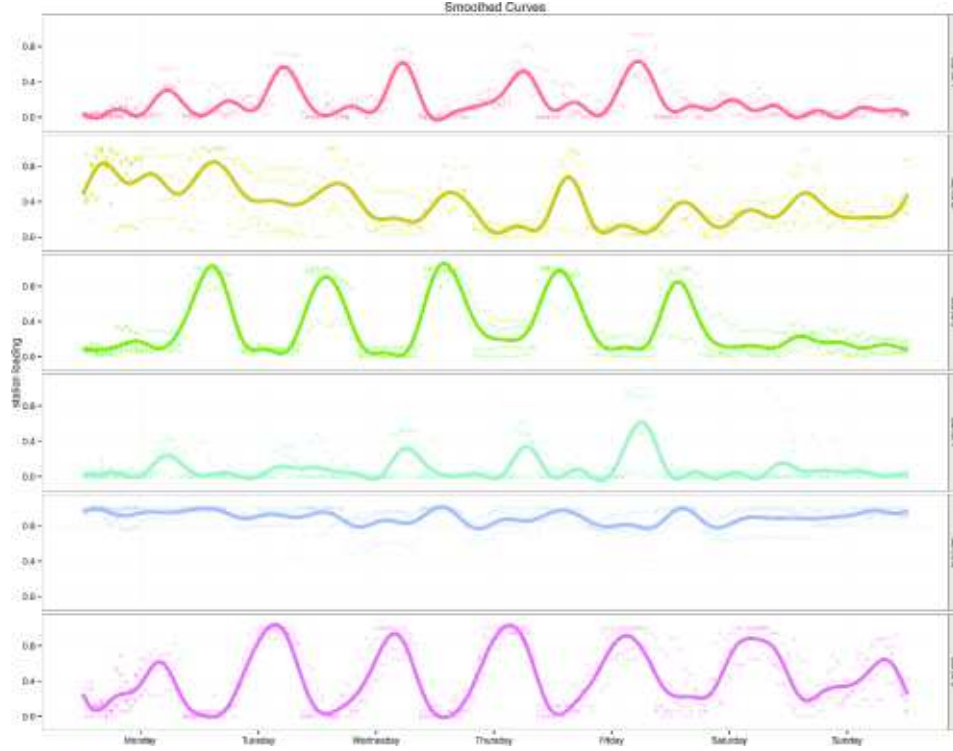


FIG. 2. Some examples of smoothed station profiles, with the corresponding observations. One month of observations is depicted here using a period of one week.

5. Our study aims, therefore, to identify the different patterns hidden in the data using functional clustering and to use them to compare the eight studied systems.

3. The discriminative functional mixture model. From a theoretical point of view, the aim of this work is to cluster a set of observed curves $\{x_1, \dots, x_n\}$ (the loading function of the bike stations) into K homogenous groups (or clusters), allowing for the analysis of the studied process. After a short review of related works in functional data clustering, this section introduces a latent functional model that adapts the model of Bouveyron and Brunet (2012) proposed in the multivariate case to functional data. An original inference algorithm for the functional model is then proposed, subsequently allowing for the clustering of the curves. The model choice and variable selection are also discussed.

3.1. Related work in functional clustering. This work is rooted in the recent advances in functional data analysis that have contributed to the development of efficient clustering techniques specific to functional data. One

of the earlier works in that domain was by James and Sugar (2003), who defined an approach that is particularly effective for sparsely sampled functional data. This method, called *fcust*, considers that the basis expansion coefficients of curves into a spline basis are distributed according to a mixture of Gaussians with cluster-specific means and common variances. The use of a spline basis is convenient when the curves are regular but are not appropriate for peak-like data, for instance, the data encountered in mass spectrometry. For this reason, Giacomini et al. (2013) recently proposed a Gaussian model on a wavelet decomposition of curves. This approach allows for addressing a wider range of functional shapes than splines. An interesting approach has also been considered by Samé et al. (2011), who assume that curves arise from a mixture of regressions based on polynomial functions, with possible regime changes at each instant of observation. Let us also mention the work of Frühwirth-Schnatter and Kaufmann (2008), who have built a specific clustering algorithm based on parametric time series models. Bouveyron and Jacques (2011) extended the high-dimensional data clustering (HDDC) algorithm [Bouveyron, Girard and Schmid (2007)] to the functional case. The resulting model assumes a parsimonious cluster-specific Gaussian distribution for the basis expansion coefficients. More recently, Jacques and Preda (2013) proposed a model-based clustering built on the approximation of the notion of density for functional variables, extended to multivariate functional data in Jacques and Preda (2014). These models assume that the functional principal component scores of curves have a Gaussian distribution whose parameters are cluster-specific. Bayesian approaches have also been proposed: For example, Heard, Holmes and Stephens (2006) consider that the basis expansion coefficients are distributed as a mixture of Gaussians whose variances are modeled by an Inverse-Gamma distribution. Further, Ray and Mallick (2006) propose a nonparametric Bayes wavelet model for curve clustering based on a mixture of Dirichlet processes.

3.2. Transformation of the observed curves. Let us first assume that the observed curves $\{x_1, \dots, x_n\}$ are independent realizations of a L_2 -continuous stochastic process $X = \{X(t)\}_{t \in [0, T]}$ for which the sample paths, that is, the observed curves, belong to $L_2[0, T]$. In practice, the functional expressions of the observed curves are not known, and we have access only to the discrete observations $x_{ij} = x_i(t_{is})$ at a finite set of ordered times $\{t_{is} : s = 1, \dots, m_i\}$. It is therefore necessary to first reconstruct the functional form of the data from their discrete observations. A common way to do this is to assume that the curves belong to a finite dimensional space spanned by a basis of functions [see, e.g., Ramsay and Silverman (2005)]. Let us therefore consider such a basis $\{\psi_1, \dots, \psi_p\}$ and assume that the stochastic process X admits

the following basis expansion:

$$(3.1) \quad X(t) = \sum_{j=1}^p \gamma_j(X) \psi_j(t),$$

where $\gamma = (\gamma_1(X), \dots, \gamma_p(X))$ is a random vector in \mathbb{R}^p , and the number p of basis functions is assumed to be fixed and known. The basis expansion of each observed curve $x_i(t) = \sum_{j=1}^p \gamma_{ij} \psi_j(t)$ can be estimated by an interpolation procedure [see Escabias, Aguilera and Valderrama (2005), e.g.] if the curves are observed without noise or by least squares smoothing if they are observed with error:

$$x_i^{\text{obs}}(t_{is}) = x_i(t_{is}) + \varepsilon_{is}, \quad s = 1, \dots, m_i.$$

The latter option is used in the present work. In this case, the basis coefficients of each sample path x_i are approximated by

$$\hat{\gamma}_i = (\Theta_i' \Theta_i)^{-1} \Theta_i' X_i^{\text{obs}},$$

with $\Theta_i = (\psi_j(t_{is}))_{1 \leq j \leq n, 1 \leq s \leq m_i}$ and $X_i^{\text{obs}} = (x_i^{\text{obs}}(t_{i1}), \dots, x_i^{\text{obs}}(t_{im_i}))'$.

3.3. The model. The goal is to cluster the observed curves $\{x_1, \dots, x_n\}$ into K homogeneous groups. Let us assume that there exists an unobserved random variable $Z = (Z_1, \dots, Z_K) \in \{0, 1\}^K$ indicating the group membership of X : Z_k is equal to 1 if X belongs to the k th group and 0 otherwise. The clustering task aims therefore to predict the value $z_i = (z_{i1}, \dots, z_{iK})$ of Z for each observed curve x_i .

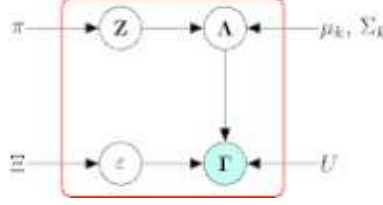
Let $F[0, T]$ be a latent subspace of $L_2[0, T]$ assumed to be the most discriminative subspace for the K groups spanned by a basis of d basis functions $\{\varphi_j\}_{j=1, \dots, d}$ in $L_2[0, T]$, with $d < K$ and $d < p$. The assumption $d < K$ is motivated by the fact that a subspace of $d = K - 1$ dimensions is sufficient to discriminate K groups [Fisher (1936), Fukunaga (1990)]. The basis $\{\varphi_j\}_{j=1, \dots, d}$ is obtained from $\{\psi_j\}_{j=1, \dots, p}$ through a linear transformation $\varphi_j = \sum_{\ell=1}^p u_{j\ell} \psi_\ell$ such that the $p \times d$ matrix $U = (u_{j\ell})$ is orthogonal. Let $\{\lambda_1, \dots, \lambda_n\}$ be the latent expansion coefficients of the curves $\{x_1, \dots, x_n\}$ on the basis $\{\varphi_j\}_{j=1, \dots, d}$. These coefficients are assumed to be independent realizations of a latent random vector $\Lambda \in \mathbb{R}^d$. The relationship between the bases $\{\varphi_j\}_{j=1, \dots, d}$ and $\{\psi_j\}_{j=1, \dots, p}$ suggests that the random vectors Γ and Λ are linked through the following linear transformation:

$$(3.2) \quad \Gamma = U\Lambda + \varepsilon,$$

where $\varepsilon \in \mathbb{R}^p$ is an independent and random noise term.

Let us now make distributional assumptions on the random vectors Λ and ε . First, conditionally on Z , Λ is assumed to be distributed according to a multivariate Gaussian density:

$$(3.3) \quad \Lambda_{|Z=k} \sim \mathcal{N}(\mu_k, \Sigma_k),$$

FIG. 3. Graphical representation for the model $\text{DFM}_{[\Sigma_k \beta]}$.

where μ_k and Σ_k are, respectively, the mean and the covariance matrix of the k th group. Second, ε is also assumed to be distributed according to a multivariate Gaussian density:

$$(3.4) \quad \varepsilon \sim \mathcal{N}(0, \Xi).$$

With these distributional assumptions, the marginal distribution of Γ is a mixture of Gaussians:

$$(3.5) \quad p(\gamma) = \sum_{k=1}^K \pi_k \phi(\gamma; U\mu_k, U^t \Sigma_k U + \Xi),$$

where ϕ is the standard Gaussian density function, and $\pi_k = P(Z = k)$ is the prior probability of the k th group.

We finally assume that the noise covariance matrix Ξ is such that $\Delta_k = \text{cov}(W^t \Gamma | Z = k) = W^t \Sigma_k W$ has the following form:

$$(3.6) \quad \Delta_k = \left(\begin{array}{cc|cc} \boxed{\Sigma_k} & \mathbf{0} & & \\ & & \beta & 0 \\ \hline \mathbf{0} & & \ddots & \\ & & 0 & \beta \end{array} \right) \left. \vphantom{\begin{array}{cc|cc} \Sigma_k & \mathbf{0} & & \\ & & \beta & 0 \\ \hline \mathbf{0} & & \ddots & \\ & & 0 & \beta \end{array}} \right\} \begin{array}{l} d \\ p-d \end{array}$$

with $W = [U, V]$, where V is the orthogonal complement of U . With this notation, and from a practical point of view, one can say that the variance of the actual data of the k th group is therefore modeled by Σ_k , whereas the parameter β models the variance of the noise outside the functional subspace. This model is referred to in the sequel as $\text{DFM}_{[\Sigma_k \beta]}$, and Figure 3 summarizes the modeling.

3.4. A family of discriminative functional model. Starting with the model $\text{DFM}_{[\Sigma_k \beta]}$ and following the strategy of Fraley and Raftery (1999), several submodels can be generated by applying constraints on the parameters of the matrix Δ_k . For instance, it is first possible to relax the constraint that the noise variance is common across groups. This generates the model

TABLE 2

Number of free parameters in covariance matrices when $d = K - 1$ for the DFM models

Model	Σ_k	β_k	Nb. of variance parameters
DFM $_{[\Sigma_k \beta_k]}$	Free	Free	$(K - 1)(p - K/2) + K^2(K - 1)/2 + K$
DFM $_{[\Sigma_k \beta]}$	Free	Common	$(K - 1)(p - K/2) + K^2(K - 1)/2 + 1$
DFM $_{[\Sigma \beta_k]}$	Common	Free	$(K - 1)(p - K/2) + K(K - 1)/2 + K$
DFM $_{[\Sigma \beta]}$	Common	Common	$(K - 1)(p - K/2) + K(K - 1)/2 + 1$
DFM $_{[\alpha_{kj} \beta_k]}$	Diagonal	Free	$(K - 1)(p - K/2) + K^2$
DFM $_{[\alpha_{kj} \beta]}$	Diagonal	Common	$(K - 1)(p - K/2) + K(K - 1) + 1$
DFM $_{[\alpha_k \beta_k]}$	Spherical	Free	$(K - 1)(K - 1)(p - K/2) + 2K$
DFM $_{[\alpha_k \beta]}$	Spherical	Common	$(K - 1)(p - K/2) + K + 1$
DFM $_{[\alpha_j \beta_k]}$	Diagonal & Common	Free	$(K - 1)(p - K/2) + (K - 1) + K$
DFM $_{[\alpha_j \beta]}$	Diagonal & Common	Common	$(K - 1)(p - K/2) + (K - 1) + 1$
DFM $_{[\alpha \beta_k]}$	Spherical & Common	Free	$(K - 1)(p - K/2) + K + 1$
DFM $_{[\alpha \beta]}$	Spherical & Common	Common	$(K - 1)(p - K/2) + 2$

DFM $_{[\Sigma_k \beta_k]}$, which is the more general model of the family. It is also possible to constrain this new model such that the covariance matrices $\Sigma_1, \dots, \Sigma_K$ in the latent space are common across groups. This submodel will be referred to as DFM $_{[\Sigma \beta_k]}$. Similarly, in each group, Σ_k can be assumed to be diagonal, that is, $\Sigma_k = \text{diag}(\alpha_{k1}, \dots, \alpha_{kd})$, and this submodel will be referred to as DFM $_{[\alpha_{kj} \beta_k]}$. The variance within the latent subspace F can also be assumed to be isotropic for each group, and the associated submodel is DFM $_{[\alpha_k \beta_k]}$. Following this strategy, 12 different DFM models can be enumerated, and an overview of them is proposed in Table 2. The table also provides, for each model, the number of variance parameters to estimate as a function of the number K of groups and the number p of basis functions. One can note that the models turn out to be particularly parsimonious because their complexity is a linear function of p , whereas most model-based approaches usually have a complexity that is a quadratic function of p .

3.5. Model inference: The FunFEM algorithm. Because the group memberships $\{z_1, \dots, z_n\}$ of the curves are unknown, the direct maximization of the likelihood associated with the model described above is intractable. In such a case, a classical solution for model inference is to use the EM algorithm. Here, however, the use of the EM algorithm is prohibited due to the particular nature of the functional subspace F . Indeed, maximizing the likelihood over the subspace orientation matrix U is equivalent to maximizing the projected variance, and it yields the functional principal component analysis (fPCA) subspace. Because F is here assumed to be the most discriminative subspace, U has to be estimated separately, and we therefore propose the algorithm described hereafter and named FunFEM. The FunFEM algorithm alternates, at iteration q , over the three following steps:

The F step. Let us first suppose that at iteration q , the posterior probabilities $t_{ik}^{(q)} = E[z_{ik}|\gamma_i, \theta^{(q-1)}]$ are known (they have been estimated in the E step of iteration $q-1$). The F step aims therefore to determine, conditionally on the $t_{ik}^{(q)}$, the orientation matrix U of the discriminative latent subspace F in which the K clusters are best separated. Following the original idea of Fisher (1936), the functional subspace F should be such that the variance within the groups should be minimal, whereas the variance between groups should be maximal. Let \mathbf{C} be the covariance operator of X with kernel

$$C(t, s) = \mathbb{E}[(X(t) - m(t))(X(s) - m(s))],$$

and \mathbf{B} be the integral between-cluster covariance operator with kernel

$$B(t, s) = \mathbb{E}[\mathbb{E}[X(t) - m(t)|Z]\mathbb{E}[X(s) - m(s)|Z]],$$

where $m(t) = \mathbb{E}[X(t)]$. In the following, and without a loss of generality, the curves are assumed to be centered, that is, $m(t) = 0$. The operator \mathbf{B} can thus be rewritten as follows:

$$\begin{aligned} B(t, s) &= \mathbb{E}[\mathbb{E}[X(t)|Z]\mathbb{E}[X(s)|Z]] \\ &= \mathbb{E}\left[\sum_{k=1}^K \mathbf{1}_{\{Z=k\}} \mathbb{E}[X(t)|Z=k] \sum_{\ell=1}^K \mathbf{1}_{\{Z=\ell\}} \mathbb{E}[X(s)|Z=\ell]\right] \\ &= \sum_{k=1}^K P(Z=k) \mathbb{E}[X(t)|Z=k] \mathbb{E}[X(s)|Z=k]. \end{aligned}$$

The Fisher criterion, in the functional case and the supervised setting [Preda, Saporta and Lévêder (2007)], looks for the discriminative function $u \in L_2[0, T]$ which is solution of

$$(3.7) \quad \max_u \frac{\text{Var}(\mathbb{E}[\Phi(X)|Z])}{\text{Var}(\Phi(X))},$$

where $\Phi(X) = \int_{[0, T]} X(t)u(t) dt$ is the projection of X on the discriminative function u . Let us recall that we consider here the unsupervised setting, and Z is an unobserved variable. The solution of (3.7) is the eigenfunction u associated with the largest eigenvalue $\eta \in \mathbb{R}$ of the following generalized eigenproblem:

$$(3.8) \quad \begin{aligned} \mathbf{B}u &= \eta \mathbf{C}u, \\ \int_{[0, T]} B(t, s)u(s) ds &= \eta \int_{[0, T]} C(t, s)u(s) ds, \end{aligned}$$

under the constraint $\langle u, \mathbf{C}u \rangle_{L_2[0,T]} = 1$. The estimator for $C(t, s)$ from the sample $\{x_1, \dots, x_n\}$, expanded on the basis $(\psi_j)_{j=1, \dots, p}$, is

$$\begin{aligned}\hat{C}(t, s) &= \frac{1}{n} \sum_{i=1}^n \left(\sum_{j=1}^p \gamma_{ij} \psi_j(t) \right) \left(\sum_{j=1}^p \gamma_{ij} \psi_j(s) \right) \\ &= \frac{1}{n} \Psi'(t) \mathbf{\Gamma}' \mathbf{\Gamma} \Psi(s),\end{aligned}$$

where $\mathbf{\Gamma} = (\gamma_{ij})_{i,j}$ is the $n \times p$ -matrix of basis expansion coefficients and $\Psi(s)$ is the p -vector of the basis functions $\psi_j(s)$ ($1 \leq i \leq n$ and $1 \leq j \leq p$). Because the variable Z is unobserved, $B(t, s)$ has to be estimated conditionally on the posterior probabilities $t_{ik}^{(q-1)} = E[z_{ik} | \gamma_i, \theta^{(q-1)}]$ obtained from the E step at iteration $q - 1$:

$$\begin{aligned}\hat{B}^{(q)}(t, s) &= \sum_{k=1}^K \frac{n_k^{(q-1)}}{n} \left(\frac{1}{n_k^{(q-1)}} \sum_{i=1}^n t_{ik}^{(q-1)} x_i(t) \right) \left(\frac{1}{n_k^{(q-1)}} \sum_{i=1}^n t_{ik}^{(q-1)} x_i(s) \right) \\ &= \frac{1}{n} \sum_{k=1}^K \frac{1}{n_k^{(q-1)}} \left(\sum_{i=1}^n t_{ik}^{(q-1)} \sum_{j=1}^p \gamma_{ij} \psi_j(t) \right) \left(\sum_{i=1}^n t_{ik}^{(q-1)} \sum_{j=1}^p \gamma_{ij} \psi_j(s) \right),\end{aligned}$$

and in a matrix form:

$$\hat{B}^{(q)}(t, s) = \frac{1}{n} \Psi'(t) \mathbf{\Gamma}' \mathbf{T} \mathbf{T}' \mathbf{\Gamma} \Psi(s),$$

with $n_k^{(q-1)} = \sum_{i=1}^n t_{ik}^{(q-1)}$ and $\mathbf{T} = (\frac{t_{ik}^{(q-1)}}{\sqrt{n_k^{(q-1)}}})_{i,k}$ is a $n \times K$ -matrix. Assuming that the discriminative function u can be decomposed in the same basis as the observed curves,

$$(3.9) \quad u(t) = \sum_{j=1}^p \nu_j \psi_j(t) = \Psi'(t) \boldsymbol{\nu},$$

the generalized eigenproblem (3.8) becomes

$$\int_{[0,T]} \frac{1}{n} \Psi'(t) \mathbf{\Gamma}' \mathbf{T} \mathbf{T}' \mathbf{\Gamma} \Psi(s) \Psi'(s) \boldsymbol{\nu} ds = \eta \int_{[0,T]} \frac{1}{n} \Psi'(t) \mathbf{\Gamma}' \mathbf{\Gamma} \Psi(s) \Psi'(s) \boldsymbol{\nu} ds,$$

which is equivalent to

$$\frac{1}{n} \Psi'(t) \mathbf{\Gamma}' \mathbf{T} \mathbf{T}' \mathbf{\Gamma} \mathbf{W} \boldsymbol{\nu} = \eta \frac{1}{n} \Psi'(t) \mathbf{\Gamma}' \mathbf{\Gamma} \mathbf{W} \boldsymbol{\nu},$$

with $\mathbf{W} = \int_{[0,T]} \Psi(s) \Psi'(s) ds$. Because this equality holds for all $t \in [0, T]$, we have

$$\mathbf{\Gamma}' \mathbf{T} \mathbf{T}' \mathbf{\Gamma} \mathbf{W} \boldsymbol{\nu} = \eta \mathbf{\Gamma}' \mathbf{\Gamma} \mathbf{W} \boldsymbol{\nu},$$

or, equivalently,

$$(3.10) \quad (\mathbf{\Gamma}'\mathbf{\Gamma}W)^{-1}\mathbf{\Gamma}'\mathbf{T}\mathbf{T}'\mathbf{\Gamma}W\boldsymbol{\nu} = \eta\boldsymbol{\nu}.$$

Finally, the basis expansion coefficient $\boldsymbol{\nu} = (\nu_1, \dots, \nu_p)'$ of the discriminative function u is the eigenvector of the above generalized eigenproblem associated with the largest eigenvalue. Once the first discriminative function, let us say u_1 , is determined, the second discriminative function is obtained by solving the generalized eigenproblem (3.10) in the complementary space of u_1 . This procedure is recursively applied until the d discriminative functions $\{u_1, \dots, u_d\}$ are obtained. The basis expansion coefficients $\boldsymbol{\nu}_j^{(q)} = (\nu_{j1}^{(q)}, \dots, \nu_{jp}^{(q)})'$, $j = 1, \dots, d$ of the estimated discriminative functions are gathered in the $p \times d$ matrix $U^{(q)} = (\boldsymbol{\nu}_{j\ell}^{(q)})_{j,\ell}$.

The M step. Following the classical scheme of the EM algorithm, this step aims to maximize, conditionally on the orientation matrix $U^{(q)}$ obtained from the previous step, the conditional expectation of the complete data log-likelihood $Q(\theta; \theta^{(q-1)}) = E[\ell(\theta; \mathbf{\Gamma}, z_1, \dots, z_n) | \mathbf{\Gamma}, \theta^{(q-1)}]$:

$$\begin{aligned} Q(\theta; \theta^{(q-1)}) &= -\frac{1}{2} \sum_{k=1}^K n_k^{(q-1)} \left[\log |\Sigma_k| + (p-d) \log(\beta) - 2 \log(\pi_k) + p \log(2\pi) \right. \\ &\quad \left. + \frac{1}{n_k^{(q-1)}} \sum_{i=1}^n t_{ik}^{(q-1)} (\gamma_i - \mu_k)^t U^{(q)} \Delta_k^{-1} U^{(q)t} (\gamma_i - \mu_k) \right] \\ &= -\frac{1}{2} \sum_{k=1}^K n_k^{(q-1)} \left[\log |\Sigma_k| + (p-d) \log(\beta) - 2 \log(\pi_k) + p \log(2\pi) \right. \\ &\quad \left. + \text{trace}(\Sigma_k^{-1} U^{(q)t} C_k U^{(q)}) + \frac{1}{\beta} \left(\text{trace}(C_k) - \sum_{j=1}^d \boldsymbol{\nu}_j^{(q)t} C_k \boldsymbol{\nu}_j^{(q)} \right) \right], \end{aligned}$$

where $\theta = (\pi_k, \mu_k, \Sigma_k, \beta)_k$, for $1 \leq k \leq K$, and $C_k = \frac{1}{n_k^{(q-1)}} \sum_{i=1}^n t_{ik}^{(q-1)} (\gamma_i - \mu_k^{(q-1)}) (\gamma_i - \mu_k^{(q-1)})^t$. The maximization of $Q(\theta; \theta^{(q-1)})$, according to π_k, μ_k, Σ_k and β , yields the following updates for model parameters:

- $\pi_k^{(q)} = n_k^{(q-1)} / n$,
- $\mu_k^{(q)} = \frac{1}{n_k^{(q-1)}} \sum_{i=1}^n t_{ik}^{(q-1)} U^{(q)t} \gamma_i$,
- $\Sigma_k^{(q)} = U^{(q)t} C_k^{(q)} U^{(q)}$,
- $\beta^{(q)} = (\text{trace}(C^{(q)}) - \sum_{j=1}^d \boldsymbol{u}_j^{(q)t} C^{(q)} \boldsymbol{u}_j^{(q)}) / (p-d)$.

Updated formula for other models of the family can be easily obtained from Bouveyron and Brunet (2012).

The E step. This last step reduces to update, at iteration q , the posterior probabilities $t_{ik}^{(q)} = E[z_{ik} | \gamma_i, \theta^{(q)}]$. Let us also recall that $t_{ik}^{(q)}$ is also the posterior probability $P(z_{ik} = 1 | \gamma_i, \theta^{(q)})$ that the curve x_i belongs to the k th component of the mixture under the current model. Using Bayes' theorem, the posterior probabilities $t_{ik}^{(q)}$, $i = 1, \dots, n$, $k = 1, \dots, K$, can be expressed as follows:

$$(3.11) \quad t_{ik}^{(q)} = \frac{\pi_k^{(q)} \phi(\gamma_i, \theta_k^{(q)})}{\sum_{l=1}^K \pi_l^{(q)} \phi(\gamma_i | \theta_l^{(q)})},$$

where $\theta_k^{(q)} = (\pi_k^{(q)}, \mu_k^{(q)}, \Sigma_k^{(q)}, \beta^{(q)})$ is the set of parameters for the k th component updated in the M step.

3.6. Model selection. We now discuss both the choice of the most appropriate model within the family and the problem of selecting the number K of groups and the intrinsic dimension d . On the one hand, it is first of interest to select the model of the DFM family that is the most appropriate to model the data at hand. On the other hand, the problem of selecting K and d can be, in fact, recast as a model selection problem. The idea here is to consider, for instance, a DFM model with $K = 2$ and the same DFM model with $K = 3$ as two different models among which one wants to choose. Thus, because a model is defined by its parametrization, its number of components K and its intrinsic dimensionality d , model selection criteria allow us to select the best combination of those three features required for modeling the data.

Classical tools for model selection include the AIC [Akaike (1974)] and BIC [Schwarz (1978)] criteria, which penalize the log-likelihood $\ell(\hat{\theta})$ as follows, for model \mathcal{M} :

$$(3.12) \quad \text{AIC}(\mathcal{M}) = \ell(\hat{\theta}) - \xi(\mathcal{M}), \quad \text{BIC}(\mathcal{M}) = \ell(\hat{\theta}) - \frac{\xi(\mathcal{M})}{2} \log(n),$$

where $\xi(\mathcal{M})$ is the number of free parameters of the model, and n is the number of observations. The value of $\xi(\mathcal{M})$ is, of course, specific to the model selected by the practitioner (cf. Table 2). Although penalized likelihood criteria are widely used, AIC and BIC are also known to be less efficient in practical situations than in simulated cases. In particular, the required regularity conditions are not fully satisfied in the mixture framework [Lindsay (1995), Ray and Lindsay (2008)] and, hence, the criteria might not be appropriate.

To overcome this drawback, Birgé and Massart (2007) recently proposed a data-driven technique, called the “slope heuristic,” to calibrate the penalty

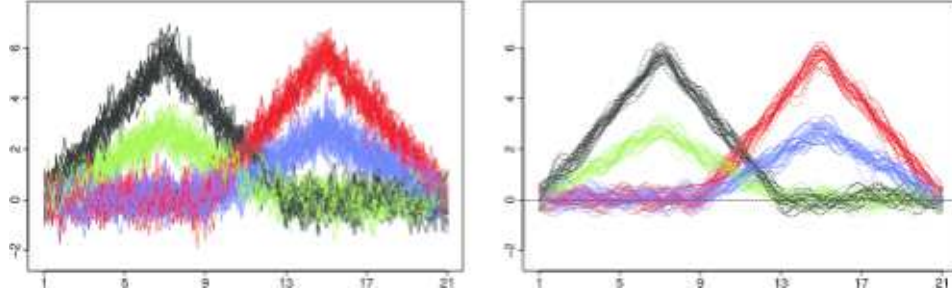
involved in penalized criteria. The slope heuristic was first proposed in the context of Gaussian homoscedastic least squares regression and was then used in different situations, including model-based clustering. Birgé and Massart (2007) showed that there exists a minimal penalty and that considering a penalty equal to twice this minimal penalty allows for approximating the oracle model in terms of risk. The minimal penalty is, in practice, estimated by the slope of the linear part when plotting the log-likelihood $\ell(\hat{\theta})$ with regard to the number of model parameters (or model dimension). The criterion associated with the slope heuristic is therefore defined by

$$(3.13) \quad \text{SHC}(\mathcal{M}) = \ell(\hat{\theta}) - 2\hat{s}\xi(\mathcal{M}),$$

where \hat{s} is the slope of the linear part of $\ell(\hat{\theta})$. A detailed overview and advice for implementation are provided in Baudry, Maugis and Michel (2012). Section 3 proposes a comparison of the slope heuristic with classical model selection criteria. In Section 4 the slope heuristic criterion is used for the model selection for the BSS data.

3.7. Selection of discriminative basis functions. Another advantage of the proposed modeling is the possibility of using the discriminative subspace to select the relevant basis functions for discriminating between the groups. Indeed, the functional subspace F allows for determining the discriminative basis functions through the loading matrix U , which contains the coefficients of the linear relation that links the basis functions with the subspace F . It is therefore expected that basis functions associated with large absolute values of U are particularly relevant for discriminating between the groups. An intuitive way to identify the discriminative basis functions would be to keep only large absolute loading variables by, for instance, thresholding. Although this approach is commonly used in practice, it has been particularly criticized by Cadima and Jolliffe (1995) because it induces some misleading information. Here, we propose selecting the discriminative basis functions by constraining the optimization problem (3.7) of the F step such that the loading matrix U is sparse (i.e., such that U contains as many zeros as possible). To this end, we follow the approach proposed by Bouveyron and Brunet (2014), who rewrite the constrained Fisher criterion as a ℓ_1 -penalized regression problem. We therefore use their algorithm [Algorithm 2 of Bouveyron and Brunet (2014)] to maximize the optimization problem (3.7) under ℓ_1 -penalization.

4. Numerical experimentations. This section presents numerical experiments to validate on simulated and benchmark data the approach presented above, before applying it on the BSS data.

FIG. 4. *Raw and smoothed simulated curves.*

4.1. *Model selection.* We first focus on the problem of model selection. Here, BIC and the slope heuristic are challenged on a set of simulated curves. A sample of $n = 100$ curves is simulated according to the following model, inspired by Ferraty and Vieu (2003), Preda (2007):

$$\begin{aligned} \text{Cluster 1: } X(t) &= U + (1 - U)h_1(t) + \varepsilon(t), & t \in [1, 21], \\ \text{Cluster 2: } X(t) &= U + (1 - U)h_2(t) + \varepsilon(t), & t \in [1, 21], \\ \text{Cluster 3: } X(t) &= U + (0.5 - U)h_1(t) + \varepsilon(t), & t \in [1, 21], \\ \text{Cluster 4: } X(t) &= U + (0.5 - U)h_1(t) + \varepsilon(t), & t \in [1, 21], \end{aligned}$$

where U is uniformly distributed on $[0, 1]$, and $\varepsilon(t)$ is white noise that is independent from U such that $\text{Var}(\varepsilon_t) = 0.5$. The functions h_1 and h_2 are defined, for $t \in [1, 21]$, by $h_1(t) = 6 - |t - 7|$ and $h_2(t) = 6 - |t - 15|$. The mixing proportions are equal, and the curves are observed in 101 equidistant points ($t = 1, 1.2, \dots, 21$). The functional form of the data is reconstructed using a Fourier basis smoothing with 25 basis functions. Figure 4 plots the simulated curves and the smoothed ones.

For each simulated data set, the number K of clusters is estimated based on both the BIC and the slope heuristic criteria. As an example of the results, Figures 5 and 6 (right panel) plot, respectively, the values of the BIC criterion and the slope heuristic for one simulation with the model $\text{DFM}_{[\Sigma_k \beta_k]}$. On this run, both criteria succeed in selecting the actual number of clusters ($K = 4$). Figure 6 may require further explanation. The left panel plots the log-likelihood function with regard to the number of free model parameters, the latter being a function of K (see Table 2). The slope heuristic consists of using the slope of the linear part of the objective function to calibrate the penalty. The linear part is here represented by the red dashed line and was automatically determined using a robust linear regression. The slope coefficient is then used to compute the penalized log-likelihood function, shown on the right panel. We can see here that the slope heuristic provides a penalty close to the one of BIC.

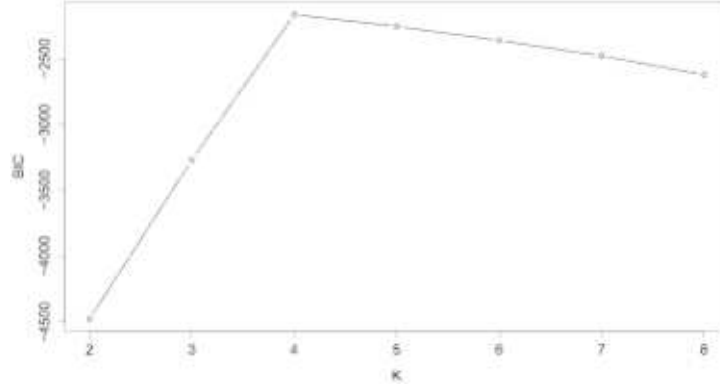


FIG. 5. Selection of the number of clusters using BIC on the simulated data (actual value of K is 4).

Both criteria were then used to select the appropriate model and number of groups on 100 simulated data sets. Tables 3 and 4 present respectively the selected number of clusters by BIC and the slope heuristic over 100 simulations for each of the 12 DFM models. It turns out that although BIC can be very efficient when the model is appropriate, it can provide unsatisfactory results in more difficult inference situations. Conversely, the slope heuristic appears to be more consistent in the selection of the number of clusters while keeping very good overall results. For this reason, the selection of models and the number of groups will be addressed in the following section with the slope heuristic.

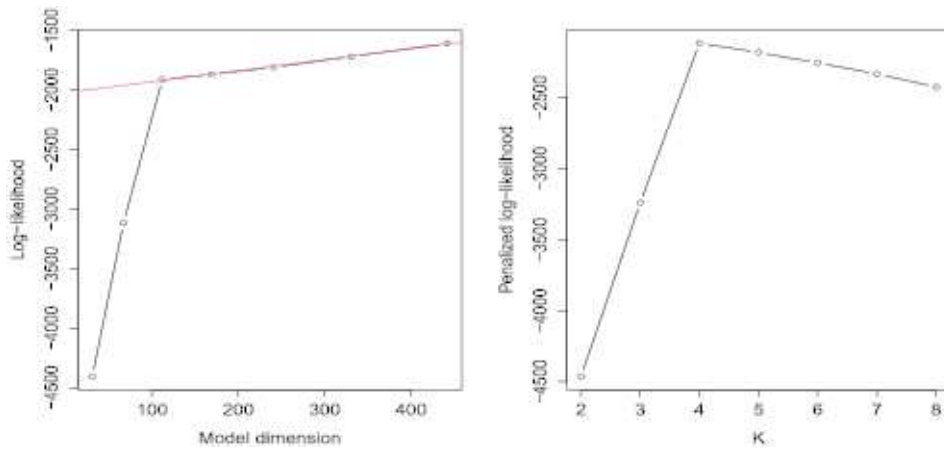


FIG. 6. Selection of the number of clusters using the slope heuristic on the simulated data (actual value of K is 4).

TABLE 3

Number of clusters selected by BIC over 100 simulations for the 12 DFM models. Actual value for K is 4

Model	Number K of clusters								
	2	3	4	5	6	7	8	9	10
DFM $_{[\Sigma_k \beta_k]}$	0	0	99	0	0	0	0	1	0
DFM $_{[\Sigma_k \beta]}$	0	0	27	37	23	12	1	0	0
DFM $_{[\Sigma \beta_k]}$	0	0	100	0	0	0	0	0	0
DFM $_{[\Sigma \beta]}$	0	0	2	2	8	10	10	10	58
DFM $_{[\alpha_{kj} \beta_k]}$	0	0	100	0	0	0	0	0	0
DFM $_{[\alpha_{kj} \beta]}$	0	0	1	5	8	12	10	7	57
DFM $_{[\alpha_k \beta_k]}$	0	0	100	0	0	0	0	0	0
DFM $_{[\alpha_k \beta]}$	0	0	0	0	1	1	4	7	87
DFM $_{[\alpha_j \beta_k]}$	0	0	100	0	0	0	0	0	0
DFM $_{[\alpha_j \beta]}$	0	0	91	5	1	1	1	0	1
DFM $_{[\alpha \beta_k]}$	0	0	100	0	0	0	0	0	0
DFM $_{[\alpha \beta]}$	0	0	97	2	1	0	0	0	0

4.2. *Selection of discriminative basis functions.* This experiment is concerned with the selection of the discriminative basis functions, that is, the most relevant ones for discriminating the clusters. In this work, the selection of the discriminative basis functions is viewed as solving the optimization problem (3.7) of the F step under sparsity constraints (i.e., such that the loading matrix U contains as many zeros as possible). To evaluate the ability

TABLE 4

Number of clusters selected by the slope heuristic over 100 simulations for the 12 DFM models. Actual value for K is 4

Model	Number K of clusters								
	2	3	4	5	6	7	8	9	10
DFM $_{[\Sigma_k \beta_k]}$	6	9	84	0	0	0	0	1	0
DFM $_{[\Sigma_k \beta]}$	15	1	81	3	0	0	0	0	0
DFM $_{[\Sigma \beta_k]}$	0	0	91	8	1	0	0	0	0
DFM $_{[\Sigma \beta]}$	0	0	77	17	5	1	0	0	0
DFM $_{[\alpha_{kj} \beta_k]}$	0	0	97	3	0	0	0	0	0
DFM $_{[\alpha_{kj} \beta]}$	0	0	65	17	14	3	1	0	0
DFM $_{[\alpha_k \beta_k]}$	0	0	85	14	1	0	0	0	0
DFM $_{[\alpha_k \beta]}$	0	0	78	14	7	1	0	0	0
DFM $_{[\alpha_j \beta_k]}$	0	1	87	11	1	0	0	0	0
DFM $_{[\alpha_j \beta]}$	0	0	67	8	6	6	4	3	6
DFM $_{[\alpha \beta_k]}$	4	0	96	0	0	0	0	0	0
DFM $_{[\alpha \beta]}$	0	0	87	6	4	2	1	0	0

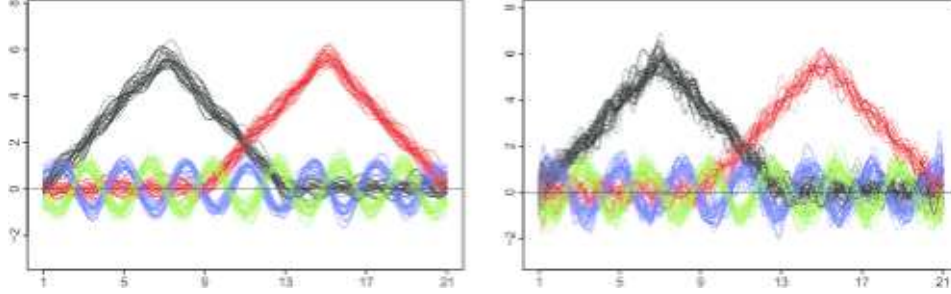


FIG. 7. *Simulated curves with cubic spline smoothing (left) and Fourier basis smoothing (right).*

of our approach to select the relevant discriminative basis functions, we consider now a simulation setting in which two primarily different frequencies are involved. The simulation setup is as follows:

$$\text{Cluster 1: } X(t) = U + (1 - U)h_1(t) + \varepsilon(t), \quad t \in [1, 21],$$

$$\text{Cluster 2: } X(t) = U + (1 - U)h_2(t) + \varepsilon(t), \quad t \in [1, 21],$$

$$\text{Cluster 3: } X(t) = U + (1 - U)\cos(2t) + \varepsilon(t), \quad t \in [1, 21],$$

$$\text{Cluster 4: } X(t) = U + (1 - U)\sin(2t - 2) + \varepsilon(t), \quad t \in [1, 21],$$

where U , $\varepsilon(t)$, h_1 , h_2 , the mixing proportions where U , $\varepsilon(t)$, h_1 , h_2 , the mixing proportions and the observation points are the same as in the previous simulation setting. The functional form of the data is reconstructed using both Fourier basis smoothing (with 25 basis functions) and a cubic spline basis (with 50 basis functions). Figure 7 plots the simulated curves, respectively smoothed on cubic splines and Fourier basis functions. Starting from the partition estimated with FunFEM and the $\text{DFM}_{[\Sigma_k \beta_k]}$ model, the sparse version of the algorithm is launched with the sparsity parameter $\lambda = 0.1$ on both Fourier and spline smoothed curves.

Figures 8 and 9 plot the selected basis functions on both spline and Fourier bases. For the Fourier basis, the selection of the basis functions indicates which periodicity in the observed curves are the most discriminative, whereas, for the spline smoothing, it indicates which time intervals are the most discriminant. On the one hand, for the Fourier basis, the sparse version of FunFEM selects only two discriminative periodicities over the 25 original basis functions (left panel of Figure 8). The selected basis functions turn out to be relevant because they actually correspond to the two periodicities present in the simulated data. The right panel of the figure plots the smoothed curves on the two selected basis functions. One can observe that the basis selection is actually relevant because the main features of the data are kept.

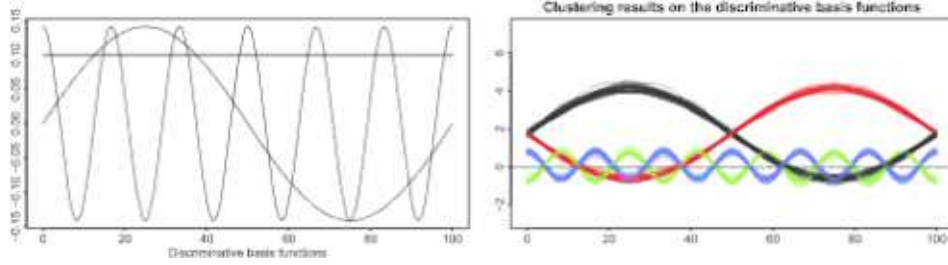


FIG. 8. *Discriminative functions among the Fourier basis functions: selected basis functions (left) and data projected on the selected basis functions (right).*

On the other hand, for the spline basis, sparse FunFEM has selected three basis functions among the 25 original ones (left panel of Figure 9). The three selected functions indicate the most discriminative time intervals. Those time intervals are reported on the right panel of the figure in addition to the curves. One can, for instance, note that the first (from the left) selected function discriminates the green clusters from the three other groups. Similarly, the second discriminative function allows for separating the black and green clusters from the blue and red curves. Finally, the last selected function aims at discriminating the black group from the others.

4.3. Comparison with state-of-the-art methods. This last numerical study aims at comparing the FunFEM algorithm with state-of-the-art methods on four real data sets that are commonly used in the functional clustering literature. The data sets considered here are as follows: the *Kneading*, *ECG*, *Face*, and *Wafer* data sets. Appendix A provides a detailed description of those data sets.

FunFEM is here compared with the six state-of-the-art methods: kmeans- d_0 and kmeans- d_1 [Ieva et al. (2013)], funclust [Jacques and Preda (2013)], funHDDC [Bouveyron and Jacques (2011)], fclust [James and Sugar (2003)]

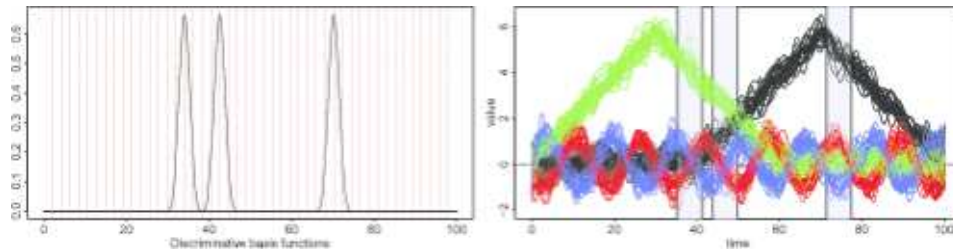


FIG. 9. *Discriminative functions among the spline basis functions: selected basis functions (left) and original data with, highlighted in grey, the time periods associated with the selected basis functions (right).*

TABLE 5

Clustering accuracies (in percentage) on the Kneading, Face, ECG and Wafer data sets for FunFEM and state-of-the-art methods. Bold results correspond to best clustering accuracies and the stars indicate the DFM model selected by BIC

Method	Kneading	ECG	Face	Wafer
kmeans- d_0	62.61	74.50	48.21	63.34
kmeans- d_1	64.35	61.50	34.80	62.53
Funclust	66.96	84.00	33.03	63.10
FunHDDC	62.61	75.00	57.14	63.41
Fclust	64.00	74.50	—	—
Curvclust	65.21	74.50	58.92	63.30
FunFEM DFM $_{[\Sigma_k \beta_k]}$	67.74	71.00	59.82	66.89
FunFEM DFM $_{[\Sigma_k \beta]}$	70.97	73.00	54.46	64.10
FunFEM DFM $_{[\Sigma \beta_k]}$	67.74	72.00	61.60	66.35
FunFEM DFM $_{[\Sigma \beta]}$	66.66	75.00	54.46	64.17
FunFEM DFM $_{[\alpha_{kj} \beta_k]}$	67.74	71.00*	53.57*	66.89
FunFEM DFM $_{[\alpha_{kj} \beta]}$	70.97	73.50	54.46	64.10
FunFEM DFM $_{[\alpha_k \beta_k]}$	67.74	71.00	53.57	66.89*
FunFEM DFM $_{[\alpha_k \beta]}$	70.97	73.00	57.14	64.10
FunFEM DFM $_{[\alpha_j \beta_k]}$	67.74	72.00	55.35	66.40
FunFEM DFM $_{[\alpha_j \beta]}$	66.66	75.00	53.57	64.17
FunFEM DFM $_{[\alpha \beta_k]}$	67.74*	72.00	53.57	66.40
FunFEM DFM $_{[\alpha \beta]}$	66.66	75.00	56.25	64.17

and curvclust [Giacofci et al. (2013)]. The two kmeans-based methods use, respectively, the L_2 -metric between curves (kmeans- d_0) and between their derivatives (kmeans- d_1). The four other methods assume a probabilistic modeling. Funclust assumes a Gaussian distribution for the functional principal components scores, whereas funHDDC, fclust and curvclust directly model the basis expansion coefficients.

Table 5 presents the clustering accuracies (according to the known labels) on the four data sets for FunFEM and the six clustering methods. FunFEM turns out to be very competitive with its challengers on those data sets. FunFEM outperforms the other methods on all data sets except the second one where it is the second best method. On the kneading, ECG and wafer sets, the improvement over state-of-the-art methods is significant. It is also worth noticing that the model selected by BIC (the model associated with the higher BIC value) often provides some of the best possible results.

5. Analysis of bike sharing systems. This section now presents the results of the application of FunFEM to one month of stock data from eight bike sharing systems (Managed by JCDecaux Ciclocity and Serco) in Europe. As explained in the [Introduction](#), clustering is a principal way to summarize the behavior of BSS stations, and this approach has already been

used in the literature. This study proposes going further here. The FunFEM algorithm presents a few advantages compared to existing works for dealing with the BSS data considered here and for comparing the eight studied systems. First, conversely to previous works, FunFEM explicitly addresses the functional nature of BSS stock data and, as we saw earlier, it outperforms multivariate and functional clustering techniques in most situations. FunFEM is therefore expected to perform well on the BSS data and to provide meaningful clusters from the operational point of view. Second, FunFEM is able to easily handle large data sets, in term of time points, due to its parsimonious modeling. This is an important point here because we consider time series over one month (1448 time points, cf. Section 2). Last but not least, FunFEM helps visualize the clustered data into a discriminative subspace. As we will see, this specific feature will be particularly informative when analyzing the clustering results on the BSS data. The visualization of the different cities within the discriminative subspace will allow us to identify the systems with operating issues and to propose practical solutions to improve those systems.

5.1. Clustering results for Paris stations. We first begin the data analysis with solely the Paris stations. The FunFEM algorithm has been applied on the data with a varying number of clusters, from 2 to 40, and using the $\text{DFM}_{[\alpha_{kj}\beta]}$ model. This model was selected based on the good results it obtained in the simulation study we performed. Note that it would also be possible to test all models and select the most appropriate one for the data using model selection. We, however, use BIC, AIC and slope heuristic criteria to choose an appropriate value for the number K of clusters. BIC and AIC provided hard-to-use values for K because even for 40 clusters, they do not reach a maximum. Conversely, the slope heuristic gave a satisfying value for K because it reaches its maximum for $K = 10$. Figure 10 shows the evolution of the log-likelihood with respect to the model dimensionality and the associated slope heuristic criterion. On the right panel, the slope heuristic criterion peaks at $K = 10$, which corresponds to an elbow in the log-likelihood function: Above this value, the gain in log-likelihood is linear with respect to the model dimensionality. This value of K was used for the cluster analysis. The mean profiles of the obtained clusters are depicted in Figure 11, together with the cluster proportions and a sample of curves that belong to each cluster.

The obtained clusters are fairly balanced, with approximately ten percent of the stations in each. The clusters are also easily distinguishable. The stations of the first two clusters get bikes during the afternoon and the evening. These stations differ during the weekend; the first cluster presents high values throughout this period, whereas the second cluster experiences a lack of bikes on Saturday mornings. Taking into account these observations,

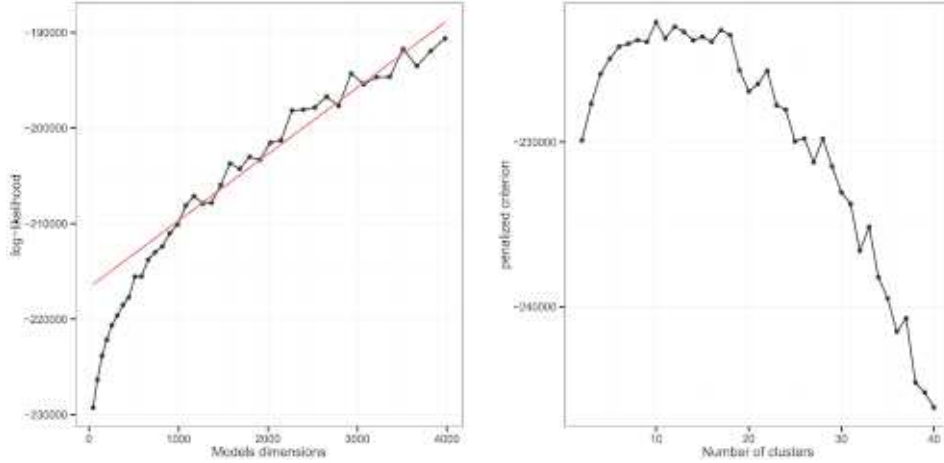


FIG. 10. Model selection plots for Paris: log-likelihood with respect to model dimensionality and its estimated linear part (left), slope heuristic criterion with respect to K (right).

we named the first cluster *Afternoon, Weekend* and the second *Afternoon* as a reference to the periods where these stations are full. The next two clusters present a phase opposition with respect to the previous ones; these stations are full at the end of the morning rush hour (approximately 9 a.m.). Because these two clusters differ in their weekend behavior, we named the first one *Morning* because these stations are almost empty throughout the entire weekend, and we named the second one *Morning, Weekend* because bikes are available at these stations for a good part of the weekend. The next two clusters do not present the same types of variations; their loading profiles are considerably stable throughout the week. The difference is in the level of fullness, with one cluster loading at approximately 0.85 and one at approximately 0.7. The first cluster also presents day variations that are not visible for the second one. We named these clusters *Full* and *Almost Full*.

Clusters 7 and 8 present overall small activity: Cluster 7 get bikes at night, but this does not saturate the stations that reach a balanced state in these time periods. This phenomenon may be due to the reallocation journey performed by the operator to balance the system at night. Cluster 8 oscillates around a balanced state, receiving slightly more bikes during the afternoons. Taking into account these remarks, we call these clusters *Night rebalancing* and *Balanced*. Finally, clusters 9 and 10 gather stations that are almost empty throughout the week. Cluster 9 presents considerably stable behavior with a constant loading profile of approximately 0.25, whereas the second one smoothly oscillates at approximately 0.1. We respectively call these clusters *Almost empty* and *Empty*.

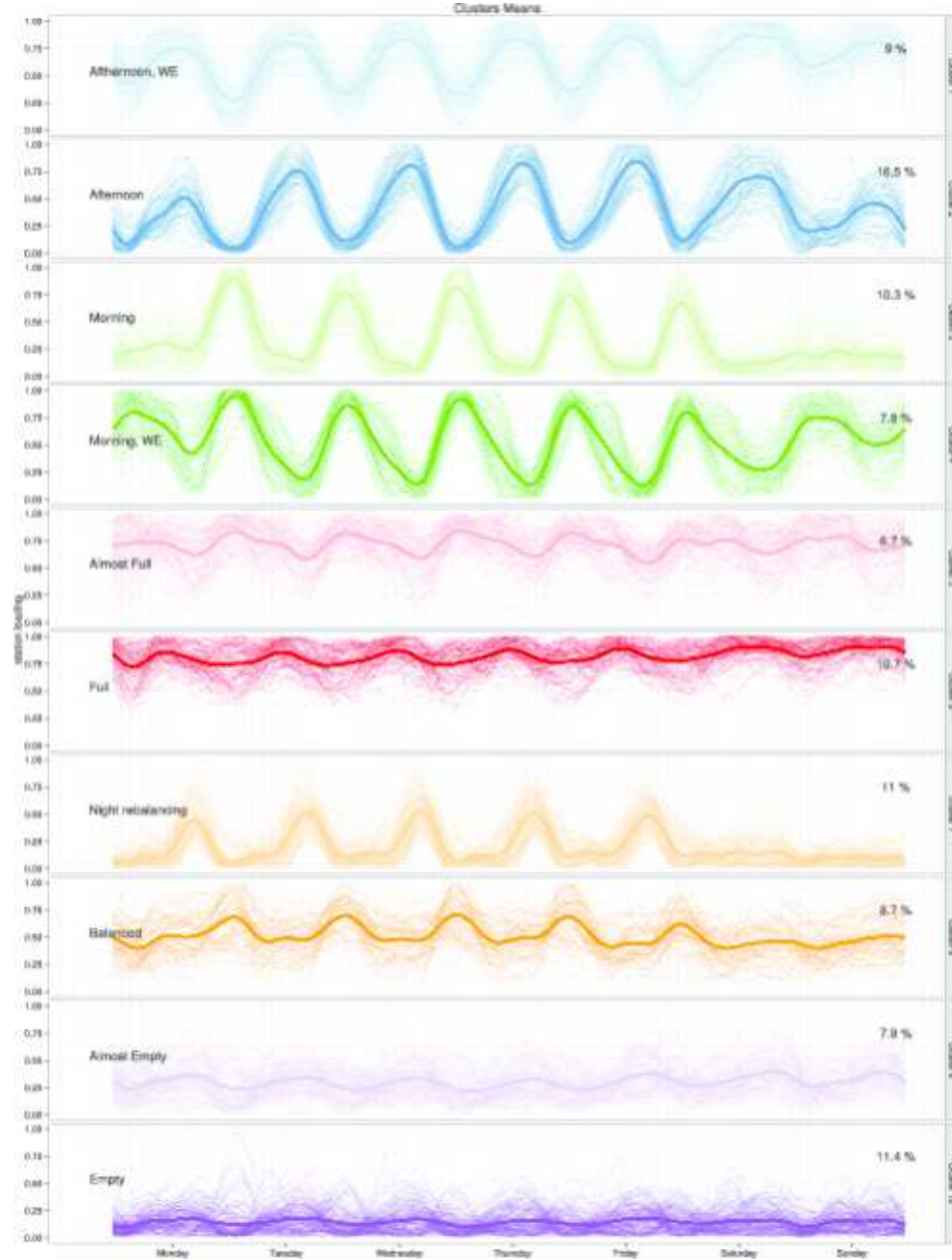


FIG. 11. Cluster mean profiles together with 1000 randomly sampled curves. The name of the clusters and their proportions are also provided.

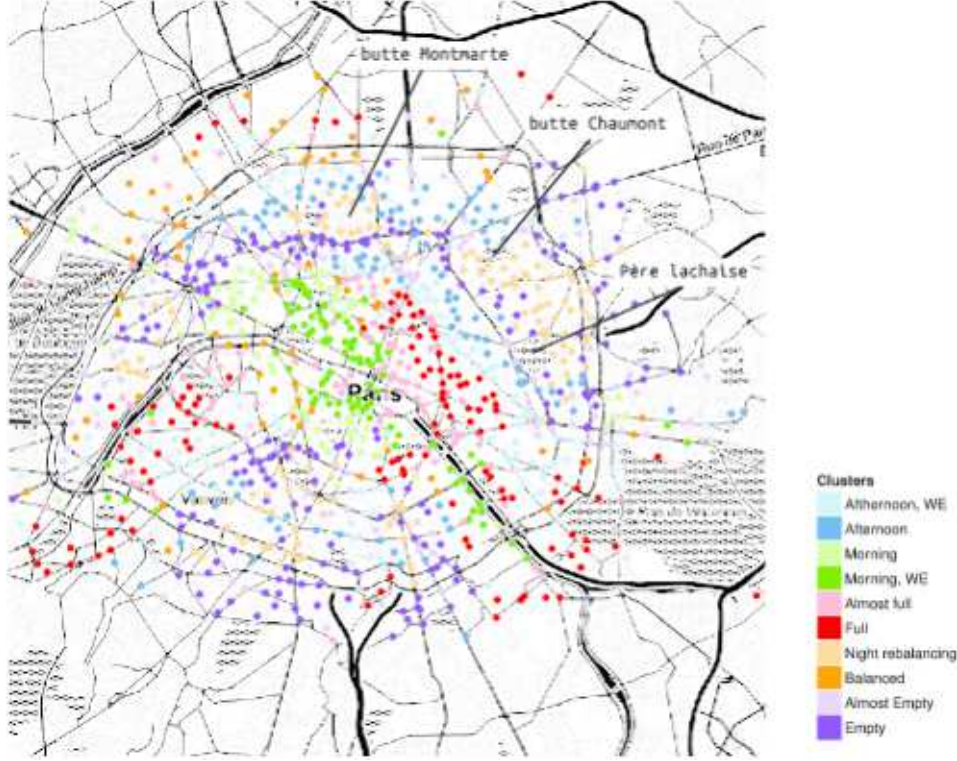


FIG. 12. Map of the clustering results for Paris stations.

To complement this analysis of the clustering results, Figure 12³ presents the spatial location of the clustering results. One of the first things that catches the eye when looking at this figure concerns the relatively good spatial organization of the results, although this information was never used in the clustering process. Stations from the same clusters are frequently grouped together on the map. From a Parisian perspective, those results are natural: The *Morning* and *Morning, Weekend* clusters (in green on the map) are located in areas with a high employment density, which therefore correspond to destinations during the morning commute. This phenomenon explains why these stations experience a saturation at the end of the morning rush hour. On the contrary, the blue clusters, which correspond to the *Afternoon* and *Afternoon, Weekend* clusters, are located in more residential neighborhoods with a higher population density. They therefore correspond to classical origins during the morning rush hour and lose their bikes during this time period. The stations that belong to these clusters are located in regions that are close to *Empty*, *Almost empty* stations, which are

³Map build using the ggmap package for R [Kahle and Wickham (2013)].

more problematic from a user perspective. These neighborhoods are not in the hyper-center of Paris, and they are also located close to stations that belong to the *Night rebalancing* cluster. The *Night rebalancing* cluster is frequently located in uphill locations, such as the “Butte Montmartre,” the “Père Lachaise” cemetery and the “Butte Chaumont” garden. Finally, the *Full* and *Almost full* stations are located in the center, whereas the *Balanced* stations are located primarily in the periphery of the system.

In comparison with previous results obtained based on Paris bike share origin/destination data, such as in Côme and Oukhellou (2014), these observations are considerably consistent. One of the major differences concerns parks and leisure locations, which do not emerge from the clustering in our study. This phenomenon may be explained by the difference in the nature of the input data. The stock data that are used in this paper do not enable the differentiation of these stations, whereas origin/destination data do. However, stock data are easier to obtain on a large scale and thus will allow cross-city comparisons, which is the subject of the next section.

5.2. Clustering results on several cities. The clustering was also performed on the entire data set, which includes stations from the eight systems (see Table 1). The same methodology was used; the curves were projected on the same Fourier basis, and, as prior, the clustering was performed with the model $\text{DFM}_{[\alpha_{kj}\beta]}$ and with a varying number of clusters, from 2 to 40. The slope heuristic leads to the same number of clusters ($K = 10$ clusters) in this larger data set. The obtained clusters are also close to those obtained only in Paris. Their profiles, which are supplied in the [Appendix](#), are close to those shown in Figure 11, and their interpretation does not differ significantly. We kept the same labels for the clusters because the main difference comes from the amplitude of the profile variations, which are smaller in the entire data set. An interesting point in the obtained results concerns the proportions of the different clusters for each city. This indeed enables an aggregate view of the systems that eases their comparison. These proportions are shown in Figure 13.

Differences between the cities are visible in this figure. The proportion of the *Night rebalancing* cluster is, for example, much more important for Paris than in any other city. This cluster, which corresponds to stations that are rebalanced during the night, is not visible in cities other than Paris. On the contrary, the proportion of the *Balanced* cluster is much smaller in Paris than in the other cities. Another clear difference concerns the *Empty* and *Almost empty* cluster stations, which are important in Marseille and Bruxelles. In Marseille, the *Full* and *Almost full* clusters are also over-represented, corresponding to more than 25% of the city stations. This system seems, therefore, the more unbalanced system with many stations frequently full

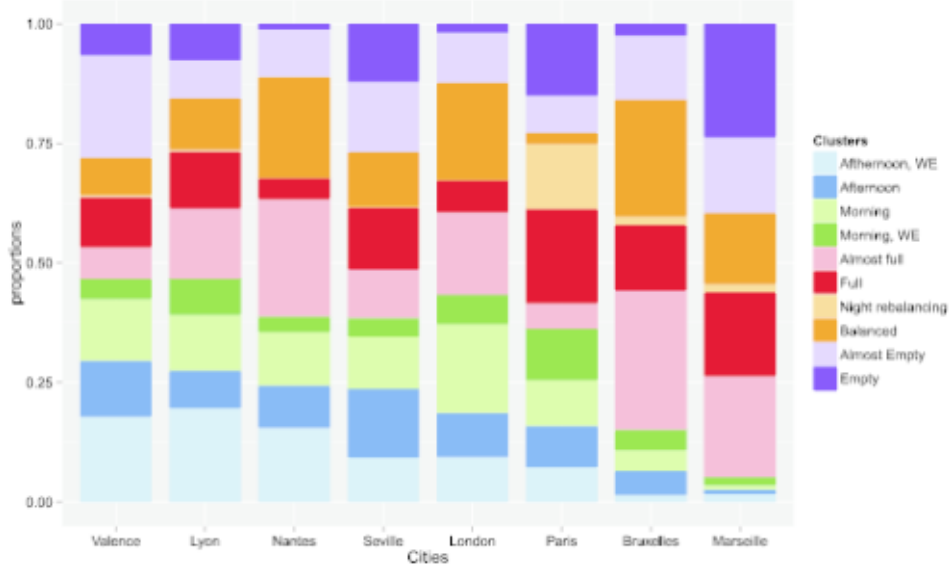


FIG. 13. Cluster proportions by city.

or empty. Conversely, the cities on the left of the plot, such as Valencia or Lyon, seem to be more active and balanced, with an important proportion of stations that belong to the *Afternoon* and *Morning* clusters. This aggregate view helps identify the BSSs that do not have satisfying behavior from the exploitation point of view. Indeed, Bruxelles and Marseille have exploitation profiles with low or even very low proportions of the active clusters (*Afternoon*, *WE*, *Afternoon*, *Morning*, *WE* and *Morning*). Conversely, the BSS of Valencia, Lyon and London seem to be the most efficient systems. Some of the factors that may explain these behaviors are the ratio between bikes and docks, the topography and geography of the cities and the bike redistribution policy.

The observations made on the cluster proportions from Figure 13 can be confirmed by looking at the discriminative subspace estimated by FunFEM. Figure 14 shows the bike stations of the 8 cities projected into the two first axes of the discriminative subspace. Figure 15 shows the projection into the third and fourth discriminative axes. The colors indicate the cluster memberships of the stations. It may first be useful to interpret the discriminative axes from the cluster meanings. The first axis puts in opposition the *Full* and *Empty* clusters and can be therefore viewed as a station loading axis. The second axis opposes the *Afternoon* and *Morning* clusters. It can therefore be linked with the phase of the curves. The third and fourth axes are less interpretable and seem primarily linked with the *Night rebalancing* cluster. Knowing the meaning of the discriminative subspace axes enables

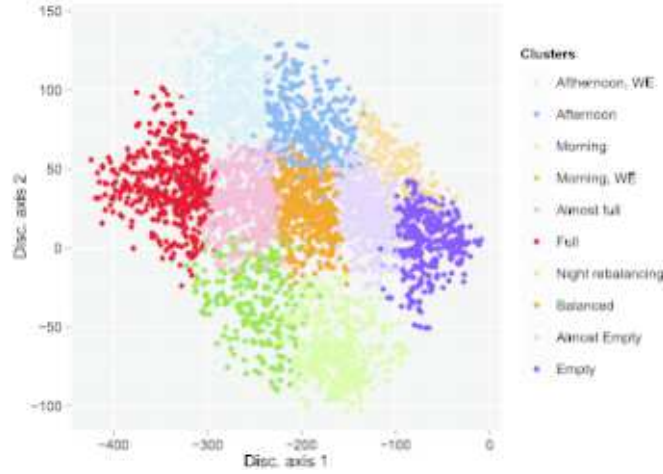


FIG. 14. *Bike stations projected into the two first axes of the discriminative functional subspace. Colors indicate the cluster memberships.*

the comparison of the studied systems through the analysis of their station behaviors. Figure 16 shows the projection of the bike stations for each city on the two first axes of the discriminative subspace. A kernel density estimation is also proposed to visualize the relative density of stations in this subspace. This visual representation confirms the first comparison results of the cluster proportions. In particular, Marseille and Bruxelles present a distribution in the discriminative subspace that is considerably different from that of other

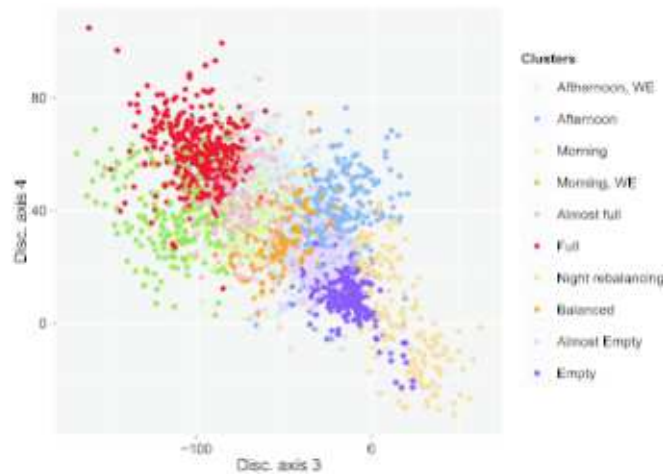


FIG. 15. *Bike stations projected into the third and fourth axes of the discriminative functional subspace. Colors indicate the cluster memberships.*

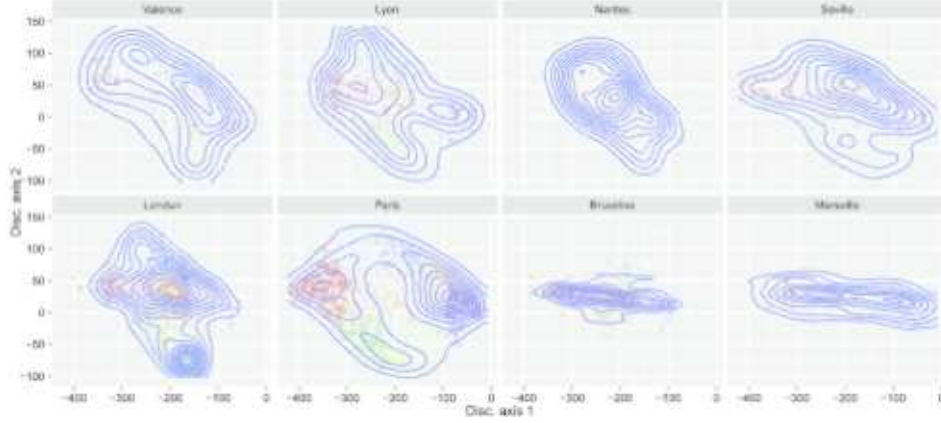


FIG. 16. *Density of bike stations per city projected into the two first axes of the discriminative functional subspace.*

cities. Indeed, both are oriented along the first discriminative axis and do not present significant variations along the second axis. The signature of those two cities within the subspace can be qualified as problematic from an operational point of view because the first discriminative axis opposes the *Full* and *Empty* clusters, whereas the second axis is associated with the *Afternoon* and *Morning* clusters.

The spatial analysis of the results was also performed by mapping the clustering results (see Figure B.2 in Appendix B). As with Paris, it turns out that the different clusters are also frequently spatially clustered. Furthermore, the same type of global organization is visible for the different cities. Stations from the *Morning* clusters are located in the center of the systems, whereas the other clusters are located in the periphery of the system.

5.3. Recommendations for BSS operators. In light of the analyses and comparisons made above, it is possible to make some recommendations for BSS operators regarding system structures and policies. On the one hand, the BSS systems of Marseille and Bruxelles appear to be composed primarily of *Full* and *Empty* stations, which necessarily implies user dissatisfaction. Possible ways to improve these situations would be either to use a “bonus” policy or to increase the rebalancing performed by the operator. The “bonus” policy is attractive for both users and providers. It consists of offering extra free minutes of bike usage to users willing to return the bike to elevated stations. In theory, this strategy should help rebalance the system. Bonus stations, for instance, are available in Paris and Bruxelles. Thanks to our discriminative subspace, it is in fact possible to check the real effect of such a policy. Figure 17 shows the density of “bonus” and regular stations within the two first axes of the discriminative functional subspace. It appears that

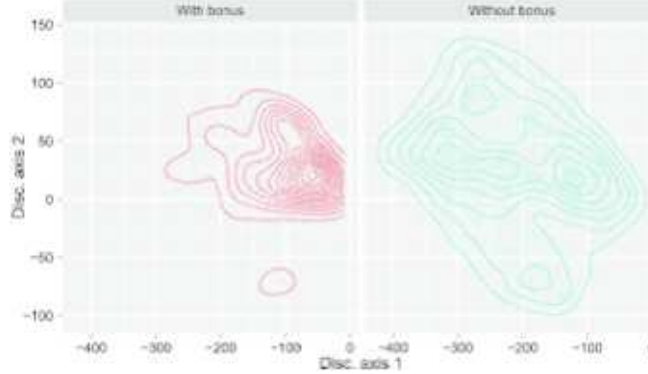


FIG. 17. Density of “bonus” (left) and regular stations (right) projected into the two first axes of the discriminative functional subspace.

the effect of the bonus policy is globally limited because there is no significant distribution difference between the regular and bonus statuses of the *Full* stations (stations projected on the left of the first discriminative axis). We therefore recommend to BSS operators to either modify their bonus policies (e.g., extra time bonus, cash reward) or to increase the nighttime rebalancing of the stations for those two cities.

However, the comparison of the largest and most efficient systems has highlighted some weaknesses of the Paris system. Although the Velib system is one of the largest and most popular systems in the world, it also appears to have too many *Full* and *Empty* stations, particularly compared to London. The night rebalancing operated by JCDecaux seems to be efficient but not sufficient to completely solve this issue. As we have seen, shared bikes are used primarily for home-work journeys, and the stations from the *Afternoon* and *Morning* clusters therefore play a key role in the system efficiency. This situation emphasizes the importance of commutes in the use of the service, and city bike policies must seriously consider this aspect when designing bike paths. London’s “Cycle Superhighways” initiative, which connects suburbs with the city center, seems particularly effective with respect to this point in our analyses. Those specific bike paths indeed connect stations from the *Afternoon* and *Morning* clusters (see Appendix B). We therefore recommend to city planners to develop bike paths in a similar way to improve the performance of system commutes.

6. Conclusion. This work was motivated by interest in analyzing and comparing several European BSSs to identify common operating patterns and to propose practical solutions to avoid potential issues. To this end, the discriminative functional mixture (DFM) model was proposed to model the

functional data generated by the systems. In this framework, the data are modeled into a discriminative functional subspace. The FunFEM algorithm has been proposed for the inference of the DFM model. The selection of the most discriminative basis functions can also be made afterward by introducing sparsity through a ℓ_1 -type penalization. Numerical experiments have demonstrated the efficiency of the proposed clustering technique for both simulated and benchmark data. FunFEM appears to be a good challenger to the best state-of-the-art methods. The numerical experiments have also shown the good behavior of the “slope heuristic” for model selection in this context.

The proposed methodology has been applied to one-month usage statistics of 8 bike sharing systems. FunFEM presents several advantages over existing works for analyzing and comparing bike sharing systems. FunFEM benefits from its parsimonious modeling and its discriminative subspace. The obtained results were easily interpretable and useful to obtain a compact representation of BSS system behaviors. In particular, the discriminative subspace appears to be a useful tool to compare the different systems with regard to the identified operating patterns. Recommendations to BSS operators are made based on the clustering results.

Finally, the discriminative subspace offers an interesting tool from an operational point of view to track changes in the behavior of bike stations. Using a sliding window and projecting the station functional description within this window into the discriminative subspace, one may obtain a trajectory for each station within the subspace, allowing for the detection of any changes in the station behavior. This may be useful when trying new pricing or bonus policies to check their effects on the system.

APPENDIX A: ADDITIONAL INFORMATION ABOUT THE BENCHMARK DATA SETS

The Kneading data set [Lévédér et al. (2004)] comes from Danone VitaPole Paris Research Center and concerns the quality of cookies and the relationship with the flour kneading process. There are 115 different flours for which the dough resistance is measured during the kneading process for 480 seconds. The data set contains 115 kneading curves observed at 241 equispaced instants of time in the interval $[0, 480]$. The 115 flours produce cookies of different quality: 50 of them produced cookies of *good* quality, 25 produced *medium* quality, and 40 produced *low* quality. Following Lévédér et al. (2004), Preda, Saporta and Lévédér (2007), least squares approximation based on cubic B-spline functions (with 18 knots) is used to reconstruct the true functional form of each sample curve. The ECG, Face and Wafer data sets are benchmarks taken from the *UCR Time Series Classification*

and Clustering website.⁴ The ECG data set consists of 200 electrocardiograms from 2 groups of patients sampled at 96 time instants and has already been studied in Olszewski (2001). The Face data set [Xi et al. (2006)] consists of 112 curves sampled from 4 groups at 350 instants of time. The Wafer data set [Olszewski (2001)] consists of 7174 curves sampled from 2 groups at 152 instants of time. For these three data sets, the same basis of functions as for the kneading data set has been arbitrarily chosen (20 cubic B-splines).

⁴http://www.cs.ucr.edu/~eamonn/time_series_data/.

APPENDIX B: DETAILED CLUSTERING RESULTS ON THE 8 BSS

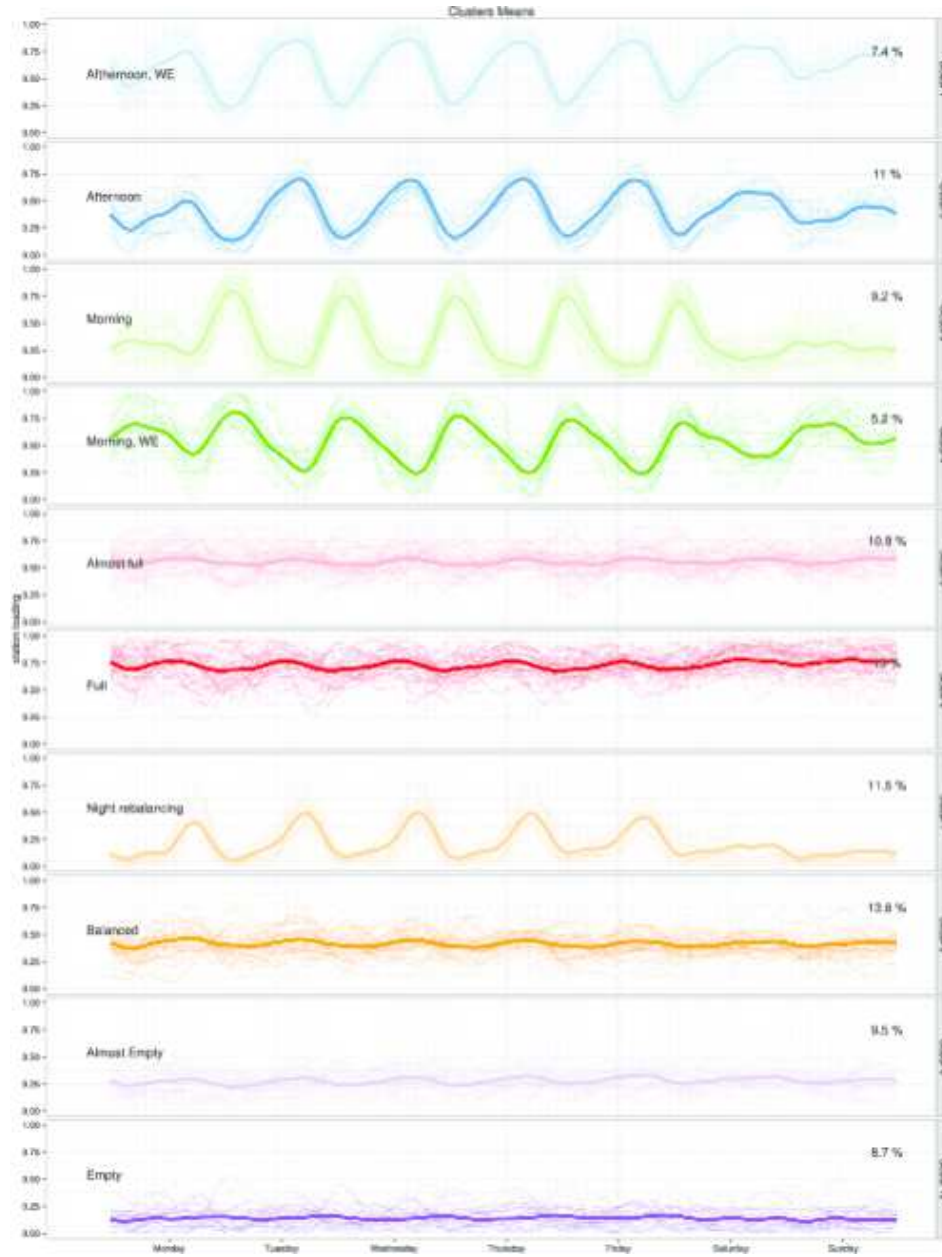


FIG. B.1. Cluster mean profiles together with 1000 randomly sampled curves for the whole data set (Paris, London, Bruxelles, Lyon, Valencia, Sevilla and Nantes).

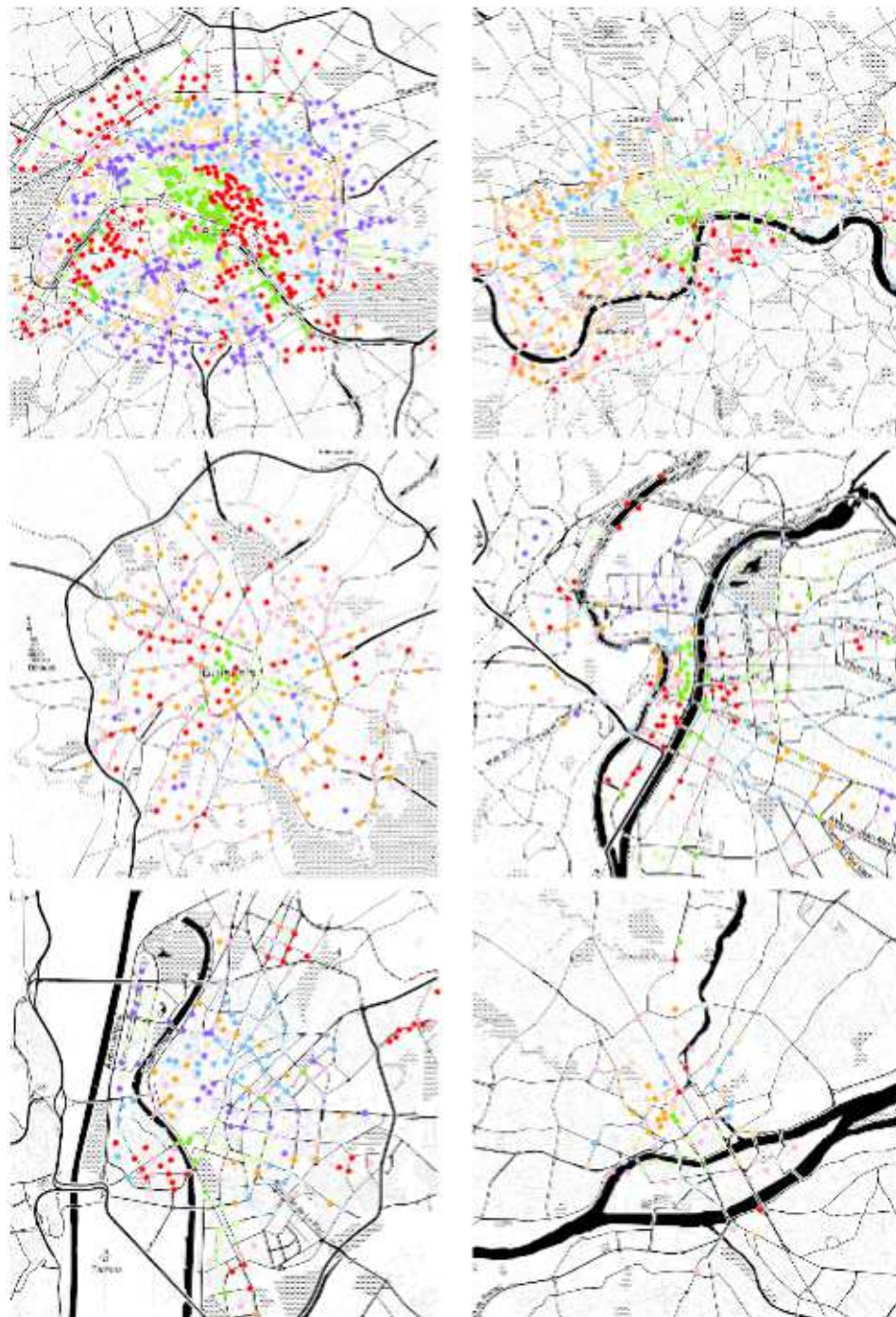


FIG. B.2. Maps of the clustering results (from left to right and top to bottom) for Paris, London, Bruxelles, Lyon, Valencia, Sevilla and Nantes.

Acknowledgments. The authors would like to thank the Editors and the reviewers for their meaningful comments which have greatly contributed to improving the manuscript.

REFERENCES

- AKAIKE, H. (1974). A new look at the statistical model identification. *IEEE Trans. Automat. Control* **19** 716–723. [MR0423716](#)
- BAUDRY, J.-P., MAUGIS, C. and MICHEL, B. (2012). Slope heuristics: Overview and implementation. *Stat. Comput.* **22** 455–470. [MR2865029](#)
- BIRGÉ, L. and MASSART, P. (2007). Minimal penalties for Gaussian model selection. *Probab. Theory Related Fields* **138** 33–73. [MR2288064](#)
- BORGNAT, P., ROBARDET, C., ROUQUIER, J. B., PARICE, A., FLEURY, E. and FLANDRIN, P. (2011). Shared bicycles in a city: A signal processing and data analysis perspective. *Adv. Complex Syst.* **14** 1–24.
- BOUYEYRON, C. and BRUNET, C. (2012). Simultaneous model-based clustering and visualization in the Fisher discriminative subspace. *Stat. Comput.* **22** 301–324. [MR2865072](#)
- BOUYEYRON, C. and BRUNET, C. (2014). Discriminative variable selection for clustering with the sparse Fisher-EM algorithm. *Comput. Statist.* **29** 489–513. [MR3261825](#)
- BOUYEYRON, C., GIRARD, S. and SCHMID, C. (2007). High-dimensional data clustering. *Comput. Statist. Data Anal.* **52** 502–519. [MR2409998](#)
- BOUYEYRON, C. and JACQUES, J. (2011). Model-based clustering of time series in group-specific functional subspaces. *Adv. Data Anal. Classif.* **5** 281–300. [MR2860102](#)
- CADIMA, J. and JOLLIFFE, I. T. (1995). Loadings and correlations in the interpretation of principal components. *J. Appl. Stat.* **22** 203–214. [MR1342655](#)
- CÔME, E. and OUKHELLOU, L. (2014). Model-based count series clustering for bike-sharing system usage mining, a case study with the Vélib system of Paris. *Transportation Research—Part C Emerging Technologies* **22** 88.
- DELL’OLIO, L., IBEAS, A. and MOURA, J. L. (2011). Implementing bike-sharing systems. In *ICE—Municipal Engineer* **164** 89–101. ICE publishing, London.
- DUDA, R. O., HART, P. E. and STORK, D. G. (2001). *Pattern Classification*, 2nd ed. Wiley, New York. [MR1802993](#)
- ESCABIAS, M., AGUILERA, A. M. and VALDERRAMA, M. J. (2005). Modeling environmental data by functional principal component logistic regression. *Environmetrics* **16** 95–107. [MR2146901](#)
- FERRATY, F. and VIEU, P. (2003). Curves discrimination: A nonparametric functional approach. *Comput. Statist. Data Anal.* **44** 161–173. [MR2020144](#)
- FISHER, R. A. (1936). The use of multiple measurements in taxonomic problems. *Annals of Eugenics* **7** 179–188.
- FRALEY, C. and RAFTERY, A. (1999). MCLUST: Software for model-based cluster analysis. *J. Classification* **16** 297–306.
- FROELICH, J., NEUMANN, J. and OLIVER, N. (2008). Measuring the pulse of the city through shared bicycle programs. In *International Workshop on Urban, Community, and Social Applications of Networked Sensing Systems. UrbanSense08* 16–20. Raleigh, NC.
- FROELICH, J., NEUMANN, J. and OLIVER, N. (2009). Sensing and predicting the pulse of the city through shared bicycling. In *21st International Joint Conference on Artificial Intelligence, IJCAI’09* 1420–1426. AAAI Press, Menlo Park, CA.
- FRÜHWIRTH-SCHNATTER, S. and KAUFMANN, S. (2008). Model-based clustering of multiple time series. *J. Bus. Econom. Statist.* **26** 78–89. [MR2422063](#)

- FUKUNAGA, K. (1990). *Introduction to Statistical Pattern Recognition*, 2nd ed. Academic Press, Boston, MA. [MR1075415](#)
- GIACOFI, M., LAMBERT-LACROIX, S., MAROT, G. and PICARD, F. (2013). Wavelet-based clustering for mixed-effects functional models in high dimension. *Biometrics* **69** 31–40. [MR3058049](#)
- HEARD, N. A., HOLMES, C. C. and STEPHENS, D. A. (2006). A quantitative study of gene regulation involved in the immune response of anopheline mosquitoes: An application of Bayesian hierarchical clustering of curves. *J. Amer. Statist. Assoc.* **101** 18–29. [MR2252430](#)
- IEVA, F., PAGANONI, A. M., PIGOLI, D. and VITELLI, V. (2013). Multivariate functional clustering for the morphological analysis of electrocardiograph curves. *J. R. Stat. Soc. Ser. C. Appl. Stat.* **62** 401–418. [MR3060623](#)
- JACQUES, J. and PREDA, C. (2013). Funchlust: A curves clustering method using functional random variable density approximation. *Neurocomputing* **112** 164–171.
- JACQUES, J. and PREDA, C. (2014). Model-based clustering for multivariate functional data. *Comput. Statist. Data Anal.* **71** 92–106. [MR3131956](#)
- JAMES, G. M. and SUGAR, C. A. (2003). Clustering for sparsely sampled functional data. *J. Amer. Statist. Assoc.* **98** 397–408. [MR1995716](#)
- KAHLE, D. and WICKHAM, H. (2013). ggmap: Spatial visualization with ggplot2. *The R Journal* **5** 144–161.
- LATHIA, N., SANIUL, A. and CAPRA, L. (2012). Measuring the impact of opening the London shared bicycle scheme to casual users. *Transportation Research Part C: Emerging Technologies* **22** 88–102.
- LÉVÉDER, C., ABRAHAM, P. A., CORNILLON, E., MATZNER-LOBER, E. and MOLINARI, N. (2004). Discrimination de courbes de prÈtrissage. In *ChimiomÈtrie 2004* 37–43.
- LIN, J. R. and YANG, T. (2011). Strategic design of public bicycle sharing systems with service level constraints. *Transportation Research Part E: Logistics and Transportation Review* **47** 284–294.
- LINDSAY, B. G. (1995). *Mixture Models: Theory, Geometry and Applications*. IMS, Hayward, CA.
- OLSZEWSKI, R. T. (2001). Generalized feature extraction for structural pattern recognition in time-series data. Ph.D. thesis, Carnegie Mellon Univ., Pittsburgh, PA.
- PRED, C. (2007). Regression models for functional data by reproducing kernel Hilbert spaces methods. *J. Statist. Plann. Inference* **137** 829–840. [MR2301719](#)
- PRED, C., SAPORTA, G. and LÉVÉDER, C. (2007). PLS classification of functional data. *Comput. Statist.* **22** 223–235. [MR2318457](#)
- RAMSAY, J. O. and SILVERMAN, B. W. (2005). *Functional Data Analysis*, 2nd ed. Springer, New York. [MR2168993](#)
- RAY, S. and LINDSAY, B. G. (2008). Model selection in high dimensions: A quadratic-risk-based approach. *J. R. Stat. Soc. Ser. B. Stat. Methodol.* **70** 95–118. [MR2412633](#)
- RAY, S. and MALLICK, B. (2006). Functional clustering by Bayesian wavelet methods. *J. R. Stat. Soc. Ser. B. Stat. Methodol.* **68** 305–332. [MR2188987](#)
- SAMÉ, A., CHAMROUKHI, F., GOVAERT, G. and AKNIN, P. (2011). Model-based clustering and segmentation of time series with changes in regime. *Adv. Data Anal. Classif.* **5** 301–321. [MR2860103](#)
- SCHWARZ, G. (1978). Estimating the dimension of a model. *Ann. Statist.* **6** 461–464. [MR0468014](#)

- VOGEL, P., GREISER, T. and MATTFELD, D. C. (2011). Understanding bike-sharing systems using data mining: Exploring activity patterns. *Procedia—Social and Behavioral Sciences* **20** 514–523.
- VOGEL, P. and MATTFELD, D. C. (2011). Strategic and operational planning of bike-sharing systems by data mining—A case study. In *ICCL* 127–141. Springer, Berlin.
- XI, X., KEOGH, E., SHELTON, C., WEI, L. and RATANAMAHATANA, C. A. (2006). Fast time series classification using numerosity reduction. In *23rd International Conference on Machine Learning (ICML 2006)* 1033–1040.

C. BOUVEYRON
LABORATOIRE MAP5
UNIVERSITÉ PARIS DESCARTES
45 RUE DES SAINTS PÈRES
75006 PARIS
FRANCE
E-MAIL: charles.bouveyron@parisdescartes.fr

E. CÔME
IFSTTAR, GRETTIA
14-20 BOULEVARD NEWTON
CITÉ DESCARTES, CHAMPS SUR MARNE
77447 MARNE LA VALLÉE CEDEX 2
FRANCE
E-MAIL: etienne.come@ifsttar.fr

J. JACQUES
LABORATOIRE ERIC
UNIVERSITÉ LUMIÈRE LYON 2
BUREAU K067
5 AV. MENDÈS FRANCE
69676 BRON CEDEX
FRANCE
E-MAIL: julien.jacques@univ-lyon2.fr